High-throughput phenotyping of *C. elegans* wild isolates reveals specific resistance and susceptibility traits to infection by distinct microsporidia species

Calvin Mok[1#], Meng A. Xiao[1*], Yin C. Wan[1*], Winnie Zhao[1], Shanzeh M. Ahmed[1], Robert Luallen[2] and Aaron W. Reinke[1#]

[1] Department of Molecular Genetics, University of Toronto, Toronto, ON, Canada

[2] Department of Biology, San Diego State University, San Diego, CA 92182, USA

*These authors contributed equally

#Corresponding authors

calvin.mok@utoronto.ca

aaron.reinke@utoronto.ca

Abstract

Animals are under constant selective pressure from a myriad of diverse pathogens. Microsporidia are ubiquitous animal parasites, but the influence they exert on shaping animal genomes is mostly unknown. Using multiplexed competition assays, we measured the impact of four different species of microsporidia on 22 wild isolates of *Caenorhabditis elegans*. This resulted in the identification of 13 strains with altered resistance or sensitivity to infection. One of these identified strains, JU1400, is sensitive to an epidermal-infecting species by lacking tolerance to infection. JU1400 is also resistant to an intestinal-infecting species and can specifically recognize and destroy this pathogen. Genetic mapping of JU1400 demonstrates that these two opposing phenotypes are caused by separate alleles. Transcriptional analysis reveals that this lack of tolerance in JU1400

results in a response that shares similarity to that induced by toxins. In contrast, we do not observe JU1400 resistance being regulated at the transcriptional level. The transcriptional response to these four microsporidia species is conserved, with *C. elegans* strain-specific differences in potential immune genes. Together, our results show that phenotypic differences to microsporidia infection amongst *C. elegans* are common and that animals can evolve species-specific genetic interactions.

Introduction

Obligate intracellular parasites only propagate inside of host cells, which places extreme pressure on the host, resulting in genomic changes [1–3]. Animals have coevolved with pathogens and genetic variation to pathogen susceptibility is common in animal populations [4,5]. Much of this genetic and phenotypic diversity to infection is specific to individual species of pathogens or even to different strains [6,7]. Hosts can evolve several ways to improve their fitness in the presence of pathogens. They can become more resistant by preventing pathogen invasion or by limiting pathogen growth [8]. Alternatively, hosts can evolve to better tolerate the infection, by limiting the negative effects of infection without reducing the amount of pathogen [9,10].

Microsporidia are a large phylum of eukaryotic obligate intracellular pathogens with a wide host range including humans and agriculturally important animals such as honey bees and shrimp [11–14]. Microsporidia infections cause developmental delays, a reduction in progeny, and increased mortality [15–17]. Several studies have shown that microsporidia can affect host population dynamics and evolution. Microsporidia have been suggested to influence the composition of *Caenorhabditis elegans* genotypes and resistant strains can outcompete sensitive ones in just a few generations [18–20]. In competition experiments with over a dozen isolates of *Daphnia magna*, different microsporidia species have been shown to select for specific strains [21,22].

Using genetic mapping, several genomic regions contributing to microsporidia resistance in *C. elegans*, *D. magna*, and honey bees have been identified [19,23–26].

C. elegans has become a powerful model for studying host-pathogen coevolution [27–30]. In the wild, *C. elegans* contend with bacterial, fungal, viral, and microsporidian pathogens and these co-evolving species represent strong selective pressures on the animal's genome [31,32]. To facilitate the study of natural diversity, hundreds of isolates of *C. elegans* have been collected from around the world [33]. These wild isolates have different levels of susceptibility to pathogens and natural variants have been discovered that impact traits such as bacterial avoidance and viral susceptibility [7,19,34–37]. Although studying phenotypic variation in wild isolates is a powerful approach, measuring each strain individually is time-consuming and laborious. To circumvent this issue, strategies have been developed to perform multiplex competitive fitness assays under selective conditions such as starvation stress or different bacterial diets [38–40]. Several approaches, termed either PhenoMIP or MIP-seq, determine the identity of these individual strains by using molecular inversion probes (MIPs) to enrich for their unique genomic signatures [39,40].

A common microbial infection found in wild *C. elegans* is from species of microsporidia in the *Nematocida* genus. Infection of *C. elegans* by microsporidia begins with ingestion of a chitin-coated spore [41]. The spore then fires its unique infectious apparatus, known as a polar tube, and deposits its sporoplasm within the host. The sporoplasm then replicates to form membrane-bound, multinucleated cells know as meronts which then differentiate into spores that are shed by the host [16]. Some *Nematocida* species, such as *N. parisii*, *N. ausubeli*, and *N. ironsii*, infect only the intestine, while others, such as *N. displodere*, *N. ferruginous*, and *N. cider*, can proliferate in several tissues including the muscle and epidermis [15,19,41–43]. *C. elegans* possess several mechanisms to defend itself against microsporidia [44,45]. Infection with microsporidia induces transcriptional upregulation of genes known as the Intracellular Pathogen Response (IPR) [46].

72 Mutations in several negative regulators of the IPR cause elevated expression of the IPR and
73 resistance to microsporidia infection [47–49]. *C. elegans* also possess a separate form of inherited
74 immunity that is activated by infection of parents and is transferred to progeny [48].

75 Here we present the results of a high-throughput fitness competition of 22 pooled *C. elegans* wild
76 isolates infected by four species of microsporidia at multiple doses. We identified 16 candidate
77 interactions of either host resistance or sensitivity. We demonstrate that the wild isolate JU1400
78 has distinct and opposing responses to infection by different microsporidia species. This strain
79 has a defect in tolerance to the epidermally-infecting *N. ferruginous* but is resistant to the
80 intestinal-infecting *N. ironsii* through specific elimination of infection by this species. Through
81 mapping experiments and the generation of recombinant strains, we demonstrate that the
82 opposing phenotypes of JU1400 are caused by separate alleles. In contrast to the species-
83 specific phenotypes we observed from fitness competitions, transcriptional analysis showed a
84 host response to infection that is mostly independent of the microsporidia species, but dependent
85 upon the *C. elegans* strain. Notably, we identified a signature of down-regulated genes that has
86 overlap with the *C. elegans* response to toxins, and this downregulated response was most
87 prominent in the tolerance-defective strain JU1400 infected with *N. ferruginous*. Our results
88 demonstrate that PhenoMIP can efficiently identify resistant and sensitive wild isolates and that
89 microsporidia genotype-specific interactions are common in *C. elegans*.

90

91 **Results**

92 ***A PhenoMIP screen of wild isolate strains reveals diverse responses to microsporidia***
93 ***infection***

94 To identify *C. elegans* strains that vary in their resistance or susceptibility to microsporidia
95 infection, we carried out a modified PhenoMIP screen. We chose 22 *C. elegans* wild isolate strains

96 that are genetically diverse and isolated from a range of geographic regions (**Supplementary**
97 **Figure S1**). We selected four pathogenic microsporidia species that differ in their impact on *C.*
98 *elegans* development and the tissues they infect (*N. parisii*, *N. ausubeli*, and *N. ironsii* infect the
99 intestine and *N. ferruginous* infects the muscle and epidermis) (**Figure 1A and Supplementary**
100 **Table S1**) [42,50–53]. We pooled equal numbers of synchronized first larval stage (L1) wild
101 isolates and a laboratory reference-derived strain (VC20019) into a single population. We then
102 plated these animals along with their food source of *Escherichia coli* bacteria mixed with one of
103 four doses of each microsporidia species (high, medium, low, and none) (**Supplementary Table**
104 **S2**). We hypothesized that a high-dose exposure could identify *C. elegans* strains that were
105 resistant or tolerant to microsporidia infection while medium- and low-dose exposures might
106 identify strains exhibiting mild to strong susceptibility to microsporidia infection. Animals were
107 exposed to microsporidia spores for 72 hours at 21°C, before collecting and adding a mixture of
108 sodium hydroxide and sodium hypochlorite to the population. This mixture inhibits microsporidia
109 from infecting the next generation of animals and synchronizes the population [48]. This
110 microsporidia-free population of L1s was then grown in the absence of infection for 72 hours at
111 21°C to allow intergenerational immunity to reset [48]. Except for the *N. ausubeli* medium-dose
112 infection replicates (**see Methods**), worms in each condition were infected for an additional three
113 cycles for a total of eight generations. Adult animals were collected every two generations at the
114 end of the uninfected phase and DNA was isolated for further analysis (**Figure 1B**).

115 To determine how population composition changes due to exposure to microsporidia, we
116 determined the relative abundance of each strain within each condition. We used MIPs to target
117 strain-specific variants for sequencing at high depth. In total we sequenced 127 samples, which
118 is the equivalent of 2162 infections and 736 mock/control infections. Combining the eight control
119 replicate sets we calculated a mean fold-change rate (FCR) as well as a modified z-score
120 distribution for each strain. Comparing this mean FCR against other replicates, we identified 16

121 nematode/microsporidia pairings with FCRs for identical replicates that were consistently +/- 1.5
122 z-scores from the mean **(Figure 2 and Table 1)**. We also generated standard growth profiles for
123 each strain in an environment free of pathogen exposure and with infection by each of the
124 microsporidia species (**Figure 3A and B**). From our analysis we observed ten interaction pairs
125 that were susceptible and six that were resistant, including the previously reported resistance
126 phenotype of CB4856 to *N. ironsii* (**Supplementary Figure S2**) [51,52]. We identified five
127 additional interactions with *N. ironsii* (ERTm5), eight with *N. ferruginous* (LUAm1), two with *N.*
128 *ausubeli* (ERTm2), and no strong interactions with *N. parisii* (ERTm1). In total, we identified 13
129 strains with phenotypes, including the strains JU360, JU1400, and MY2 that had interactions with
130 more than one species of microsporidia (**Figure 2 and Table 1**).

131 **JU1400 fails to tolerate *N. ferruginous* infection**

132 To validate a subset of our large-scale multiplex identification of microsporidia-strain phenotypes,
133 we performed isogenic population infection experiments. We infected individual strains with doses
134 of microsporidia spores equivalent to those used in the PhenoMIP experiment (**Figure 3C and D**
135 **and Supplementary Figures S3-S5**). We examined a combination of phenotypes including
136 morphology of adult populations, formation of microsporidia meronts or spores, and embryo
137 production. Most resistant strains tended to experience a smaller reduction in embryo production
138 compared to lab reference N2. Susceptible strains, on the other hand, experienced developmental
139 delay phenotypes and/or a reduction in fecundity – both of which would contribute negatively to
140 the fitness readout observed by PhenoMIP. These phenotypes were most evident in JU1400 and
141 MY1 which both had severe, dose-dependent responses to infection by the epidermal
142 microsporidia species *N. ferruginous* (**Figure 3C and D and Supplementary Figure S6**). In total,
143 of the 12 pairs that we tested (**Table 1**), nine had a reduction in embryos that could account for
144 the fitness changes observed from our PhenoMIP screen. Additionally, of the eight pairs we

145 retested that had a z-score over 2.5, seven had a significant reduction in embryos when infected,
146 compared to N2.

147 To examine how a *C. elegans* strain responds to different microsporidia species, we focused on
148 JU1400, in which we observed interactions with both *N. ferruginous* and *N. ironsii*. To determine
149 why JU1400 is sensitive to *N. ferruginous*, we performed pulse-chase experiments by infecting
150 animals for 3 hours, washing away free spores, and replating animals for an additional 69 hours
151 [51]. We observed that the percentage of JU1400 and N2 animals infected with *N. ferruginous*
152 was similar (**Figure 3E and Supplementary Figure S7A and B**). Additionally, the amount of
153 meronts formed during infection did not significantly differ between N2 and JU1400 (**Figure 3F**
154 **and Supplementary Figure S7C and D**). Taken together, these results demonstrate that
155 although JU1400 is more sensitive to the effects of *N. ferruginous*, JU1400 is not significantly
156 more infected, suggesting a defect in tolerance.

157 To determine the specificity of JU1400 to *N. ferruginous* infection, we infected JU1400 with other
158 related microsporidia species and strains. We infected JU1400 with a second isolate of *N.*
159 *ferruginous,* LUAm3, as well as a separate muscle and epidermal-infecting microsporidian, *N.*
160 *cider* [43]. Infection by LUAm3 caused the same severe phenotype as LUAm1 (**Supplementary**
161 **Figure S8A and B**). JU1400 is infected by *N. cider* to a similar extent as N2, but infection by this
162 species resulted in a dose-dependent reduction in embryo numbers in JU1400 that was not
163 observed in N2 (**Supplementary Figure S8C and D**).

164 **JU1400 specifically clears *N. ironsii* infection**

165 In addition to susceptibility to *N. ferruginous,* we also observed a fitness disadvantage in JU1400
166 to high-dose exposures of *N. ironsii* in our PhenoMIP screen (**Figure 3A**). When we infected
167 JU1400 with *N. ironsii* for 72 hours, we observed no significant difference in the normalized
168 number of embryos between N2 and JU1400 (**Figure 4A**). However, JU1400 is much less

169 infected, suggesting that JU1400 is resistant to *N. ironsii* infection **(Figure 4C and**
170 **Supplementary Figure S9A and C)**. To determine whether there was a fitness advantage at a
171 later time point, we exposed JU1400 animals to *N. ironsii* for 96 hours and observed significantly
172 more embryos and significantly less infection compared to N2 (**Figure 4B and D and**
173 **Supplementary Figure S9B and D**). Together our data suggest that although JU1400 appears
174 to have a short-term disadvantage in our pooled competition assays, in the long-term this strain
175 has an advantage due to enhanced resistance towards *N. ironsii*.

176 Several mechanisms of *C. elegans* resistance to microsporidia infection have been described,
177 including a block of invasion or clearance of infected parasite [48,51,52,54]. To determine how
178 JU1400 is resistant to *N. ironsii* infection, we performed a pulse-chase experiment by infecting
179 animals for 3 hours, washing away any external microsporidia spores, and examining animals at
180 3, 24, and 72 hours post infection (hpi). Both N2 and JU1400 had similar number of sporoplasms
181 at 3 hpi, but JU1400 had decreased levels of pathogen at both 24 and 72 hpi (**Figure 5A**). This
182 experiment revealed that JU1400 does not block microsporidia invasion, but instead has the
183 capability to actively eliminate *N. ironsii* infection. To determine if the resistance in JU1400 was
184 also dependant upon development stage, we performed pulse-chase infections at the L4 stage
185 and observed that JU1400 animals could no longer clear the infection (**Figure 5B**).

186 Resistance to *N. ironsii* has previously been observed in the *C. elegans* CB4856 strain [51]. This
187 resistance has been shown to occur through a modest decrease in invasion and the ability to
188 clear the infection at the L1 stage. To compare the properties of these two resistant strains, we
189 infected both strains with *N. ironsii* for 72 hours. This experiment shows that JU1400 is more
190 resistant to infection **(Figure 5C**). To determine the specificity of JU1400 resistance, we tested
191 infection with either *N. parisii* or *N. ausubeli* for 72 hours. CB4856 was slightly, but not significantly
192 less infected by *N. parisii* and *N. ausubeli,* whereas JU1400 was infected by these species to the
193 same extent as N2 (**Figure 5D**). We also tested the ability of JU1400 and CB4856 to clear

194 microsporidia infection, and both strains could only eliminate *N. ironsii* (**Supplementary Figure**
195 **S9E and F**). Together, these results demonstrate that JU1400 resistance is specific to *N. ironsii*.

196 The immunity of JU1400 against *N. ironsii* could be because JU1400 specifically recognizes *N.*
197 *ironsii* infection and induces broad immunity towards microsporidia or the immunity itself could be
198 specific for *N. ironsii*. To distinguish between these possibilities, we set up coinfection
199 experiments using species-specific FISH probes and then coinfected JU1400 and N2 animals
200 with *N. ausubeli* and either *N. ironsii* or *N. parisii*. Under these conditions, *N. ironsii* sporoplasms
201 are eliminated regardless of the presence of *N. ausubeli*. There is no clearance of *N. ausubeli*
202 observed, either by itself or in the presence of *N. ironsii*. (**Figure 5E and Supplementary figure**
203 **S10A and B**). No clearance was observed in N2 regardless of the infection condition
204 (**Supplementary Figure S10C**). These results further demonstrate that JU1400 has specific
205 immunity towards *N. ironsii*.

206 ***Genetic mapping reveals multiple loci are responsible for the interactions of JU1400 with***
207 ***microsporidia***

208 The opposing phenotypes of JU1400 in response to microsporidia infection could be caused by
209 the same or different genetic loci. To determine the genetic basis for JU1400 being sensitive to
210 *N. ferruginous* and resistant to *N. ironsii*, we mapped the causative alleles using a pooled
211 competitive fitness assay [55]. We crossed JU1400 to the mapping strain VC20019 and infected
212 F2 animals with either *N. ferruginous* for 72 hpi or *N. ironsii* for 96 hpi **(Supplementary Table**
213 **S3**). After two rounds of selection, genomic DNA was isolated from each sample and MIP-MAP
214 sequencing libraries were generated [55]. As a control, we used this approach to map the
215 resistance of CB4856 to *N. ironsii.* We then compared our results to a previous study that
216 determined regions responsible for resistance [51]. Although the previous mapping study was
217 based on pathogen load as opposed to our mapping measuring a competitive fitness advantage,

218 several regions on chromosome II and the right arm of chromosome V are in agreement with each
219 other (**Supplementary Figure S11)**.

220 Our mapping results of JU1400 with *N. ferruginous* identified a single peak of VC20019 marker
221 fixation on the left-hand side of chromosome I (**Figure 6A**). This mapping was repeated with MY1,
222 another strain with a fitness disadvantage with *N. ferruginous* **(Figure 3B-D)**. The region being
223 selected against was the same in MY1, although this strain also carries the z*eel-1/peel-1*
224 incompatibility locus at chromosome I which accounts for the specific signal seen at the
225 I:2,726,021 marker in both the infected and uninfected samples (**Supplementary Figure S12A)**
226 [56]. To determine if the same locus was responsible for *N. ferruginous* in MY1 and JU1400, we
227 tested their ability to complement. First, we determined that both MY1 and JU1400 display a
228 recessive phenotype when crossed to our control strain. We then mated MY1 and JU1400 and
229 the resulting cross progeny were susceptible to *N. ferruginous* infection, indicating that the two
230 strains do not complement (**Supplementary Figure S13A and B**). We then infected MY1 with *N.*
231 *ironsii*. Although there were slightly fewer MY1 animals containing spores compared to N2, we
232 did not observe any difference in meront numbers, and JU1400 animals had less spores or
233 meronts than MY1 (**Supplementary Figure S13C and D**). This result is consistent with our
234 PhenoMIP data which did not indicate a strong interaction between MY1 and *N. ironsii* **(Figure**
235 **3B and Figure 2).** Together this data suggests a region on the left side of chromosome I is
236 responsible for sensitivity to *N. ferruginous* in several strain*s*.

237 Our mapping of JU1400 with *N. ironsii* identified three regions that are linked with resistance to
238 infection, one on the left-hand side of chromosome II from 1,639,865-4,426,687, a second in a
239 broad area of chromosome V from 11,035,658-18,400,066, and a third on the right-hand side of
240 chromosome X from 15,180,772-17,676,467 (**Figure 6B**). A similar pattern was observed when
241 these mapping experiments were performed at 72 hours, with the exception that the region on
242 chromosome X was no longer observed (**Supplementary Figure S12B**). We also observed a

243 region on the left side of chromosome I where JU1400 variants were selected against upon
244 infection. Together, our data suggests that JU1400 resistance to *N. ironsii* is multigenic and can
245 be influenced by infection time.

246 To confirm that the region on chromosome I was responsible for sensitivity to *N. ferruginous*
247 infection, we generated Near Isogenic Lines (NIL). These NILs were constructed by crossing a
248 version of N2 that contained GFP integrated on chromosome I (AWR133) (**Supplementary**
249 **Figure S14A**). We tested eight independent NILs that contained at least some JU1400 sequence
250 to the left of I:2,851,000. All eight of these NILs were sensitive to infection by *N. ferruginous*
251 (**Supplementary Figure S14B).** We used molecular markers to genotype these NILs, mapping
252 the susceptibility locus to I:1-1,051,810 (**Supplementary Table S4**). We then outcrossed one of
253 these NILs, AWR140 back to N2 six times. During this outcrossing process, we recovered two
254 lines, AWR144 and AWR145, that contained different responses to *N. ferruginous* infection
255 (**Figure 6D**). We performed whole-genome sequencing of AWR138 (another independently
256 isolated NIL), AWR140, AWR144, and AWR145 which narrowed the critical region of association
257 for our phenotype to I:1-701,078 (**Figure 6C**). Within this region, we identified 68 protein-coding
258 variants across 41 genes. The NIL AWR145 is sensitive to *N. ferruginous* infection but is only
259 partially resistant to infection by *N. ironsii* (**Figure 6D and E).** Together, our data demonstrate
260 that the *N. ferruginous* sensitivity and *N. ironsii* resistance to JU1400 are determined by distinct
261 genetic loci.

262 ***Transcriptional analysis of the JU1400 response to microsporidia infection***

263 To determine how the JU1400 strain differs in its response to microsporidia infection, we
264 performed transcriptional analysis. We grew three biological replicates of N2 and JU1400 L1
265 stage animals either without microsporidia or infected with one of *N. parisii*, *N. ironsii*, *N.*
266 *ferruginous*, or *N. ausubeli* for 48 hours. We then extracted and sequenced the *C. elegans* and
267 microsporidia mRNA. First, we mapped the microsporidia mRNA in each of the eight infected

268 samples. For the three intestinal infecting species, between ~1-9% of reads were mapped for
269 each sample, with the exception of *N. ironsii* in JU1400, where few reads were identified, which
270 is consistent with this strain being resistant to this species. For *N. ferruginous*, fewer reads were
271 observed in either strain compared to the intestinal species, which is consistent to what we
272 observed by microscopy (**Supplementary Figure S15 and Supplementary Table S5**).

273 We then sought to determine how the two strains responded to the four different microsporidia
274 species (**Supplementary Table S6)**. First, we used principal component analysis, which
275 accounted for about half of the variance observed in the data and revealed a clear clustering
276 between the two strains (**Figure 7A and Supplementary Figure S16**). Second, we clustered the
277 differential expression profiles of the eight infected samples. This approach revealed several large
278 groups of genes that were differentially expressed either across most samples or within the same
279 strain **(Figure 7B** and **Supplementary Table S7).** Although the largest difference in the samples
280 is between the two strains, we observe significant correlation between strains infected with each
281 microsporidia species (**Supplementary Figure S17**).

282 We then determined the properties of genes that are differentially regulated in each sample**.** The
283 number of differentially upregulated or downregulated genes ranged from 6-819, with the most
284 being in JU1400 infected with *N. ferruginous* **(Figure 7C).** We then classified differentially
285 expressed genes into either conserved, microsporidia species specific, strain specific, or species-
286 strain specific categories **(Figure 7D)**. We identified 97 genes upregulated in all samples, and no
287 genes that were broadly downregulated. We identified ~30-50 differentially expressed genes
288 specific to either *N. ausubeli* or *N. ferruginous* infection, one gene specific to *N. parisii* infection,
289 and no genes specific to *N. ironsii* infection. We also observed 45 or more differentially
290 upregulated genes that were specific to either N2 or JU1400. To determine the types of
291 differentially expressed genes in these samples, we annotated them using a set of domains
292 previously observed to be regulated during microsporidia infection [46,47,57] (**Supplementary**

293 **Table S8)**. About 35% of the conserved response were genes containing these domains, with the
294 most frequent being PALS, F-box, and MATH/BATH domains. About 25% of the strain specific
295 genes also contained these domains, with each strain having at least one PALS, F-box, and
296 MATH/BATH, c-type lectin, and skr domain- containing gene expressed that is specific to that
297 strain **(Figure 7D)**. Skp-related proteins (*skr*) in *C. elegans* were shown to bind to CUL-6 to
298 ubiquitylate specific proteins[58]. *skr-4* is upregulated in both host strains infected by all
299 microsporidia species. Among the upregulated genes, we also observe strain specific *skr* genes
300 such as JU1400 specific *skr-6*, and N2 specific *skr-5* (**Supplementary Table S7)**.

301 To understand how transcriptional responses correlated with resistant and susceptible
302 phenotypes, we analyzed genes that were specifically regulated in JU1400 when infected with
303 either *N. ironsii* or *N. ferruginous* **(Figure 7D)**. Surprisingly, we only observed three differentially
304 expressed genes specific to *N. ironsii* infection of JU1400. In contrast, we saw 181 upregulated
305 and 266 down-regulated genes specific to *N. ferruginous* infection of JU1400. Many of the
306 upregulated genes contained domains enriched in the IPR. The down-regulated genes contained
307 a few genes with IPR domains, as well as 23 genes with cuticle collagen domains. These proteins
308 with collagen domains were especially striking, as we never identified more than one of these
309 genes having altered expression in any of the other gene sets.

310 To determine if other stresses had similarities to the response of JU1400 to *N. ferruginous*, we
311 compared the set of genes specifically differentially expressed in this sample to previously
312 published *C. elegans* transcriptional datasets [59]. We identified the top ten chemical or microbial
313 treatment data sets that had the most significant overlap with JU1400 infected with *N. ferruginous*
314 (**Supplementary Table S9)**. We then determined the overlap of these data sets to all our samples
315 (**Figure 7E and Supplementary Table S10).** This revealed that genes differentially
316 downregulated in JU1400 in response to *N. ferruginous* infection overlapped significantly with
317 treatments of chemical poisons such pesticides (fenamiphos and dichlorvos), organic compounds

318 (acrylamide and tert-butyl hydrogen peroxide), and the heavy metals (mercury and cadmium). All
319 of these treatments have been shown previously to inhibit the development or the production of
320 progeny in *C. elegans* [60–63]. We also observed significant overlap of the response to these
321 chemicals with JU1400 infected with *N. ironsii*, and both strains infected with *N. ausubeli*. These
322 three infected samples along with JU1400 infected with *N. ferruginous* also contained the largest
323 number of significantly down regulated genes (**Figure 7C and Supplementary Figure S18).**
324 Additionally, we observed significant overlap of these four microsporidia infected samples to
325 pathogenic bacteria or toxins including *Staphylococcus aureus*, *Serratia marcescens*, *Bacillus*
326 *thuringiensis*, *Xenorhabdus nematophila*, and *Pseudomonas aeruginosa* (**Figure 7F**). These
327 patterns of transcriptional overlap were the most striking with differentially downregulated genes,
328 although some overlap with upregulated genes was also observed (**Supplementary Figure S19**).

329 **Discussion**

330 Animal populations often have genetic diversity to bacterial, viral, and fungal pathogens, but less
331 is known about how microsporidia influences host variation [5,6]. To investigate how different
332 microsporidia species impact genetic diversity, we measured the phenotypic responses to
333 infection in a collection of genetically diverse *C. elegans* wild isolates. A total of 13 out of 22
334 strains displayed a significant difference in sensitivity or resistance to infection compared to the
335 population. We detected interactions with three of the four microsporidia species we measured,
336 with *N. ironsii* and *N. ferruginous* accounting for most of the sensitive and resistance interactions
337 observed.

338 So far, the causative gene for any host variants that influence microsporidia interactions has not
339 been identified. Previous genetic mapping in *C. elegans*, *D. magna*, and honey bees have
340 revealed 3-6 loci involved in resistance and sensitivity to microsporidia [19,23–26]. Additionally,
341 some loci in *D. magna* appear to be specific to different microsporidia species, which we show to
342 be the case for JU1400 [24]. Our genetic analysis of JU1400 identified that susceptibility to *N.*

343 *ferruginous* in both JU1400 and MY1 mapped to a single region on the left arm of chromosome I
344 while the resistance phenotype of JU1400 to *N. ironsii* appears to be caused by at least three
345 genomic regions. Taken together, our results add to the increasing evidence that suggests that
346 microsporidia have had a major impact on the evolution of animal genomes.

347 Microsporidia infect a wide diversity of animal phyla and infections are highly prevalent [12,13,64].
348 Nine species of microsporidia have been reported to infect *C. elegans*, with four having been
349 found in wild isolates and five capable of infecting *C. elegans* after isolation of microsporidia from
350 other nematode species [15,19,41,65]. The most common are the intestinal-infecting *N. parisii*
351 and *N. ausubeli,* which have been found in Europe, the United States, India, and Africa. The
352 geographical relationships between the strongest interactions we detected is not clear; JU1400
353 was isolated in Spain, *N. ironsii* in Hawaii, and *N. ferruginous* in France. Although host genetic
354 factors were shown to be responsible for the geographic range of a microsporidian infecting *D.*
355 *magna*, further work is needed to understand if there is a geographic basis to microsporidia
356 resistance and susceptibility in *C. elegans* [66].

357 Pathogen tolerance is being increasingly appreciated as a valuable way for hosts to improve
358 fitness in the presence of pathogens, though these mechanism are less understood [67]. Here we
359 show that JU1400 is very sensitive to infection by two different epidermal infecting microsporidian
360 species, but this strain does not have significantly higher levels of *N. ferruginous* than non-
361 sensitive control strains. RNA-seq analysis reveals that JU1400 has a unique response to
362 microsporidia when infected with *N. ferruginous*. This response shares similarities to several
363 chemical toxins and pathogens that have been shown to damage *C. elegans*. This signature is
364 also detected to a lesser extent in other strain-species pairings that cause developmental delay,
365 including *N. ausubeli* with either strain or *N. ironsii* with JU1400 [50]. Further work uncovering the
366 genetic variant responsible for this aberrant response will help elucidate the mechanistic basis of
367 tolerance to microsporidia infection.

368 JU1400 is resistant to *N. ironsii* infection by clearing the invaded parasite. This immune
369 mechanism is similar to previous results seen in *N. ironsii* infection of CB4856. However, the
370 immunity in JU1400 results in less infection than in CB4856. Additionally, the fitness gain
371 observed in JU1400 occurs at a later time point. The JU1400 resistance mechanism is specific,
372 as the clearance we observe does not occur in even the closely related sister species *N. parisii*,
373 which shares 92% identical DNA [42]. A strain of mosquito that is resistant to infection by a
374 parasitic nematode was shown to rely on activation of an upregulated immune response [68].
375 However, we see no evidence for an increased transcriptional response of JU1400 in response
376 to *N. ironsii*. A potential caveat to these experiments is that we infected JU1400 at the L1 stage,
377 but measured the transcriptional response at the L4 stage, a stage where if infections are initiated,
378 parasite clearance is not observed. We do observe additional parasite clearance between the L3
379 and adult stages, suggesting that if there was transcriptional signature of resistance, it would be
380 observed under our experimental conditions. Instead of a specific transcriptional response of
381 JU1400 to *N. ironsii*, we observe a *C. elegans* strain-specific response of immune genes including
382 upregulation of several CHIL genes, which have been observed to be upregulated in response to
383 epidermally infecting oomycetes, but have not previously been observed in response to
384 microsporidia infection [69,70]. This strain specific-response of *C. elegans* has also been
385 observed with several bacterial pathogens, suggesting that there exists a diversity of innate
386 immune responses within the *C. elegans* population [71]. We also observe more strain-specific
387 regulated genes than species-specific regulated genes, suggesting that *C. elegans* responds
388 similarly to infection by different species of *Nematocida* [72].

389 Here we demonstrate that PhenoMIP can be used to identify variants of pathogen infection in a
390 high-throughput manner. The genomic loci responsible for these phenotypes can then be
391 identified using MIP-MAP [73]. We only tested a small fraction of the current *C. elegans* isotypes
392 identified, suggesting there is much variation to microsporidia within *C. elegans*. Our pooled

393 selection approach could also be applied to other *C. elegans*-related microbes such as those
394 isolated from the *C. elegans* microbiome or known pathogens and viruses [74,75]. Here we
395 studied the animal's reproductive fitness, but our approach could be modified to select for
396 pathogen load using fluorescently labelled pathogens. The wild isolate collections of *C. elegans*
397 provide a unique opportunity to study how animals evolve in response to infection. Coupling this
398 collection with a high-throughput sequencing approach for variant identification is likely to be
399 fruitful in discovering and elucidating the evolved mechanisms of host-responses in coevolving
400 pathogens.

401 **Acknowledgements**

402 We thank Hala Tamim El Jarkass for providing helpful comments on the manuscript. We thank
403 John Calarco for the kind gift of plasmids to perform CRISPR and Robert Waterston and Donald
404 Moerman for the kind gift of reagents to perform PhenoMIP and MIP-MAP. This work was
405 supported by Canadian Institutes of Health Research grants no. 400784 and 461807 and an
406 Alfred P. Sloan Research Fellowship FG2019-12040 (to A.W.R.). Some strains were provided by
407 the CGC, which is funded by NIH Office of Research Infrastructure Programs (P40 OD010440)
408 and we thank WormBase.

409 **Author contributions**

410 C. M. and A. W. R. conceived of the project. C. M., M. A. X., Y. C. W., and A.R.W. designed and
411 analyzed the experiments and cowrote the paper, with consolation from all the authors. C. M., M.
412 A. X., W.Z., and S. M.A. conducted experiments. R. J. L. provided novel reagents. A.W.R.
413 provided funding and mentorship.

414 **Competing Interests**

415 The authors declare that they have no competing interests.

416

417 **Methods**

418 ***Nematode maintenance and worm pooling***

419 Nematode strains were maintained at 21°C on a modified version of nematode growth media
420 NGM) with a 1:1 ratio of Agar:Agarose to reduce burrowing by wild isolate strains. NGM plates
421 were seeded with OP50-1 bacteria grown to saturation overnight in lysogeny broth (LB) at 37°C
422 and concentrated to 10X. All wild isolate strains used (**Supplementary Data S1**) are available
423 from the CGC. The AWR133 mapping strain was generated from VC20019 by inserting a GFP at
424 I:2,851,135 using CRISPR-based homologous recombination [76]. Nematode strains were grown
425 continuously without any starvation or contamination for a minimum of two weeks before seeding
426 individual strains to two 15-cm NGM plates seeded with 1.5 ml of 40X concentrated OP50-1. After
427 96 hours, gravid adult populations were bleach-synchronized [77] and allowed to hatch into axenic
428 M9 media for ~16 hours at 20°C. Synchronized L1 samples were counted and equal numbers of
429 animals were mixed into a single population before redistributing ~13,000 L1s to each 15-cm
430 NGM experimental plate with a mixture of 1.5 ml of 40X OP50-1 and the appropriate amount of
431 spores as needed (See **Supplementary Table S2**).

432 ***PhenoMIP competitive assays***

433 PhenoMIP competitive assays were based on a previously described protocol [39]. We modified
434 this method to use bleach-synchronization between generations to directly measure egg-
435 production as an output of population fitness. At each generation, samples were bleach-
436 synchronized as gravid adults ~72 hours after plating L1s and incubating at 21°C. Bleached
437 embryos were then allowed to hatch over 18-22 hours while incubating on a shaker at 21°C in
438 axenic M9 media. Each sample was gently pelleted and 3 – 7 µl of each pellet was used to seed
439 the experimental plate for the next generation of animals. Overall, the competitive assay consisted

440 of four total cycles, with one infection generation and one rest generation per cycle. For each
441 infection cycle, 3 ml of 40X OP50-1 culture was mixed in 15-ml falcon tubes with twice the
442 indicated dose of spores used on each infection experiment before splitting the mixture to each
443 duplicate plate. Worm populations for each specific replicate were then added to the plate and
444 samples were distributed evenly across the NGM surface before drying. For each rest cycle, worm
445 pellets were plated onto 15-cm NGM plates previously seeded with 1.5 ml of 40X OP50-1 culture.
446 Prior to bleach-synchronizing the 72h-resting generation, a subsample of the population was
447 collected and frozen as a genomic DNA source. Microsporidia doses were adjusted after the first
448 infection round in order to ensure high enough selection pressure throughout the population
449 without causing the populations to become completely infertile or developmentally arrested
450 (**Supplementary Table 2**) [78]. The Initial infection round with *N. ausubeli* caused animals on the
451 high-dose plates to produce no progeny. Therefore, the medium-dose infection series became
452 the high-dose series at 53,000 spores/cm^2. A new medium-dose series was started using an
453 uninfected control replicate population from the first rest-phase. This new medium-dose series
454 (39,800 spores/cm^2) therefore only experienced three rounds of infection selection of *N. ausubeli*.

455 ***PhenoMIP sequencing and analysis***

456 PhenoMIP sequencing libraries were generated using previously designed MIPs for the wild
457 isolate strains [39]. Individual MIPs were normalized to a concentration of 100 µM and pooled to
458 a maximum volume of 85 µl. 10 µl of 10X Polynucleotide Kinase (PNK) Buffer and 5 µl of PNK
459 were added to a volume of 85 µl pooled MIPs before incubating for 45 minutes at 37°C and 20
460 minutes at 80°C. This pool was then diluted to a working concentration of 330 nM. Libraries were
461 generated using 160 ng of genomic DNA from each sample and generated as previously
462 described [55]. Libraries were sequenced on an Illumina NextSeq system with each PhenoMIP
463 library ranging between 0.0882×10^6 and 2.723×10^6 reads and a mean of 9566 ± 7994 reads per
464 probe.

465 For each sequencing library, reads were initially analysed as previously described [55] with the
466 exclusion of the normalization step for each MIP. After abundance of each MIP was calculated,
467 an average abundance was calculated for each strain as well as a standard deviation across this
468 average. These values were used in downstream analysis of population structure across multiple
469 timepoints.
470
471 Population structure and fold-change analysis was calculated across each experiment using the
472 amalgamated data from above. Strains with a starting abundance value below $5x10^{-3}$, CB4854
473 and JU312, were eliminated from downstream population analysis. Remaining data were further
474 transformed with any values below $1.0x10^{-3}$ being converted to this value to accommodate log_2
475 growth analysis. Total fold-change and mean fold-change were calculated based on starting and
476 end-point changes in abundance versus total generations (two generations per infection cycle).
477 In samples with negative trajectories, however, the final generation of growth was calculated as
478 the first instance of abundance at or below the lower limit of $1.0x10^{-3}$. Mean fold-change rate was
479 calculated based on the total fold-change abundance in the final generation of growth divided by
480 the expected number of generations passed. Each experimental condition may have had multiple
481 biological replicates (referred to in text as replicates), each with a time-series of samples. Each
482 fold-change rate calculated for a single time-series represented a single replicate. Mean fold-
483 change rate for each strain was therefore a combination of multiple replicates across multiple
484 experimental conditions (**Supplementary Data S1**).
485
486 Given the nature of the smaller datasets and the expectation of potential outliers stretching out
487 the tails of the mean FCR distribution, modified z-scores were calculated using the following
488 formula where $\tilde{Y}$ is the median of the data and $MAD = median(|Y_i - \tilde{Y}|)$
489

490 $$M_i = \frac{0.6745(x_i - \tilde{x})}{MAD}$$

491

492 To identify outliers and potential interaction candidates, we used a minimum z-score of ± 1.5 as
493 our threshold where both replicate samples were each required to meet the threshold.

494 ***Microsporidia infection assays***

495 Continuous microsporidia infection assays were conducted using ~1,000 bleach-synchronized
496 L1s obtained from cultures rotating at 21°C for 18-22 hours. Worm populations were pre-mixed
497 in a 1.5 ml microfuge tube with 300 µl of 10X OP50-1 and microsporidia spores (**Supplementary**
498 **Table S2**). Samples were then spread onto individual unseeded 6-cm NGM plates and allowed
499 to dry before incubating at 21°C. Plate populations were imaged using a
500 Leica S9 i Stereomicroscope before fixing samples for microscopy. Animals were washed in
501 M9/0.1% Tween-20 at least three times before fixing with acetone. Chitin staining for
502 microsporidia and embryos was performed using Direct Yellow 96 [50]. Meronts and sporoplasms
503 were visualized using FISH probes conjugated to CAL Fluor Red 610 (LGC Biosearch
504 Technologies). *N. ferruginous* was stained using 3 ng/ul of a mix of three CAL Fluor Red 610
505 probes designed to target the 18S rRNA: GTTGCCCGCCCTCTGCC,
506 CTCTGTCCGTCCTCGGCAA, and CGGTCTCTAATCGTCTTC. For species specific staining,
507 MicroF-CAL Fluor Red 610 (AGACAAATCAGTCCACGAATT) was used for *N. parisii* and
508 Microsp1A-FAM (CAGGTCACCCCACGTGCT) was used for *N. ausubeli*. Unless otherwise
509 noted, all remaining FISH probes used 5 ng/µl of MicroB, a *Nematocida* microsporidia 18S rRNA
510 sequence: CTCTCGGCACTCCTTCCTG [53]. Stained samples were mixed with Biotium
511 EverBrite mounting medium with DAPI before mounting on slides for quantitation.

512 ***Microscopy and image quantification***

513 All imaging was done using an Axio Imager.M2 (Zeiss) and captured via ZEN software under
514 identical exposure times per experiment. Animals containing clumps of spores visible in the body
515 after 72 hours by DY96 straining were considered as 'new spore formation'. Animals with one
516 sporoplasm or more in intestinal cells stained with FISH were considered infected. Gravidity of
517 worms was determined by counting the number of embryos per hermaphrodite animal.

518 Pathogen burden and body size was determined using ImageJ/FIJI software [79]. Individual
519 worms were outlined as "region of interest" with selection tools. Body size of worms were
520 determined using the "measure area" function. To quantify fluorescence (pathogen burden),
521 signal from FISH staining was subjected to the "threshold" function followed by "measure percent
522 area" tool.

523 ***Pulse-chase assays***

524 Pulse-chase assays were performed on 6-cm NGM plates with roughly 6,000 bleach-
525 synchronized L1s obtained from cultures rotating at 21°C for 18-22 hours. Worm populations were
526 first premixed in a 1.5 mL microcentrifuge tube with 5 µL of 10X OP50-1 and 1.25 million spores
527 per microsporidia strain. This dose was chosen to produce N2 controls with 85-90% infection
528 rates at 3 hpi. Samples were then spread onto individual unseeded 6-cm NGM plates and allowed
529 to dry before incubating at 21°C for 3 hours. Plates were then washed at least two times with M9
530 in a 1.5mL microcentrifuge tube to remove OP50-1 and residual spores. Half the population was
531 then fixed in acetone and stored at -20°C. The other half was mixed with 50 µL of 10X OP50-1
532 and plated onto 6-cm NGM plates. Samples were then incubated at 21°C for 21 hours (24hpi),
533 washed, fixed, and replated (with 300 µL of 10X OP50-1) in the same manner as described above.
534 The plates were incubated at 21°C for 48hours (72hpi) before washing and fixing in acetone.
535 Pulse-chase co-infection assays were performed as described above, except samples were
536 infected with either one or two species of microsporidia for 24 hours total. Pulse-chase assays
537 initiated at the L4 stage were performed by using ~3000 bleach-synchronized L1s mixed with 200

538 µL of 10X OP50-1 and plated on unseeded 6-cm NGM plates for 48 hours. Worm populations
539 were then washed two times with M9 in 1.5 mL microcentrifuge tubes. 50 µL of 10X OP50-1 and
540 spores were added to each worm population and then plated on unseeded 6-cm NGM plate for 3
541 hours at 21°C. Samples were then washed and replated as described above. Chitin and FISH
542 staining were performed as described above for all pulse-infection experiments.

543 ***MIP-MAP and variant analysis***

544 Wild isolates were mapped using a competitive fitness approach after crossing with males of the
545 mapping strain AWR133, a CRISPR-inserted Pmyo-2::GFP version of VC20019. Mapping was
546 completed using 2-4 competitive selection cycles on 1- cm NGM plates. Each cycle consisted of
547 2 generations of recombinant populations, each added to plates as bleach-synchronized L1
548 animals. In the first generation ~10,000 L1 cross-progeny animals were exposed to continuous
549 microsporidia infection (See **Supplementary Table S3**) for ~72 hours before bleach-
550 synchronizing. Next, ~8,000 L1s were plated within 24 hours to "rest" on OP50-1-seeded NGM
551 plates and grown for ~72 hours before being bleach-synchronized. L1 progeny of the "rest" phase
552 were then plated onto both an OP50-1-seeded plate with spores to begin the next cycle and a
553 secondary plate without spores to generate a sample to collect genomic DNA. Genomic samples
554 were prepared with 250 ng of genomic DNA and VC20019 MIP-MAP library probes as previously
555 described[55]. Sequencing libraries were run on an Illumina NextSeq, with 161,054-801,840
556 reads per library and a mean of 4005 ± 2760 reads per MIP across the entire data set.

557 **Near isogenic lines construction**

558 Near isogenic lines were tracked across chromosome I using four markers located at four
559 locations matching sequenced variants identified in JU1400: cewivar00066519 (491,763),
560 cewivar00067570 (1,051,810), cewivar00069114 (1,567,450), and cewirvar00070489
561 (2,012,869). These markers were used for restriction fragment length polymorphism analysis with

562 the enzyme DraI. JU1400 hermaphrodites were crossed with AWR133 males. F1 GFP+ animals
563 at the L4 stage were chosen to produce F2 animals. 48 GFP+ animals were chosen and screened
564 at marker cewivar00066519 for JU1400 homozygosity and further screened at cewirvar00070489
565 for JU1400 homozygosity or heterozygosity. Seven F2 lines were chosen based on their
566 genotyping and four of these gave rise to five main progenitor NILs, each of which was used to
567 create a separate GFP+ and GFP- NIL strain. In total 10 NILs were generated and tested for
568 susceptibility against LUAm1. One line was chosen for outcrossing (AWR140) which gave rise to
569 the AWR144 and AWR145 NILs.

570 ***C. elegans* WGS Analysis**

571 Worm strains used for WGS were grown on 10-cm plates with OP50-1 for 3 days and allowed to
572 starve. Plates were then washed at least two times with M9 in microcentrifuge tubes before
573 freezing in liquid freezing solution and then stored at -80C. gDNA was then extracted and
574 quantified with Qubit™ HS system. gDNA quality was determined by agarose gel electrophoresis
575 and photometric OD260/280 of 1.8-2.0. gDNA was submitted to The Centre for Applied Genomics
576 (TCAG) for library preparation and whole genome sequencing on an Illumina HiSeq 2500 SR50
577 Rapid Run flowcell in pools of six samples per lane. Raw sequencing reads of each NIL were
578 aligned to the N2 reference of the WBcel215 release (accession: PRJNA13758) using bowtie2
579 [80]. Then, samtools was used to convert it into .bam format and freebayes was used to perform
580 variant calling with the default settings [81,82]. The breakpoints between VC20019 and JU1400
581 in chromosome I of each NIL were computed and visualised using vcf-kit [83].

582 **RNA extraction and mRNA sequencing**

583 Infection samples for mRNA sequencing were prepared by mixing ~10,000 bleach-synchronized
584 L1 stage animals with 1mL of 20X OP50-1 and 10 million *N. parisii* spores, 10 million *N. ausubeli*
585 spores, 10 million *N. ironsii* spores, and 30 million *N. ferruginous* spores in four separate

586 microcentrifuge tubes. Samples were then spread onto individual NGM plates and allowed to dry
587 before incubating at 21°C for 48 hours. Samples for RNA extraction were washed in M9/0.1%
588 Tween-20 in 15mL conical tubes at least three times before adding 1mL of TRI-Reagent® (Sigma-
589 Aldrich). Total RNA extraction and ethanol precipitation protocols was performed as per Tri-
590 Reagent® manufacturers instruction. Libraries were prepared using NEBNext® Ultra™ II
591 Directional RNA Library Prep Kit for Illumina® kit as per manufacturer's instruction. RNA
592 sequencing was carried out using Illumina NovaSeq-SP flow cell by The Centre for Applied
593 Genomics (TCAG).

594 **Microsporidia RNA-seq analysis**

595 Using Bowtie2 v2.4.4, indexes were built from *Nematocida parisii* strain ERTm1 (Genbank:
596 GCF_000250985.1), *Nematocida ausubeli* strain ERTm2 (Genbank: GCA_000738915.1),
597 *Nematocida parisii* strain ERTm5 (Genbank: GCA_001642415.1) and *Nematocida ferruginous*
598 strain LUAm1 (Accession: JALPMW000000000) The genome annotation file of each *Nematocida*
599 species was converted into gtf format using Gffread v0.12.3. Paired end reads were aligned to
600 corresponding index and genome annotation files using TopHat v2.1.2. Cufflinks v2.2.1 was used
601 to generate a transcriptome assembly for each sample, which was then combined with the
602 corresponding reference genome annotation using Cuffmerge of the Cufflinks 2.2.1 package to
603 produce a single annotation file.

604 ***C. elegans* mRNA-seq analysis**

605 The paired end reads generated for each strain were submitted as separate projects to Alaska
606 v1.7.2 (http://alaska.caltech.edu), which is an online automated RNA-seq analysis tool in
607 collaboration with Wormbase. Briefly, Bowtie2 [80], Samtools [81], RseQC [84], FastQC, and
608 MultiQC [85] were used for quality control of the input files. Kallisto [86] was used for the read
609 alignment and quantification, followed by differential analysis by Sleuth. For both N2 and JU1400

610 samples, the reads were aligned to the N2 reference of the WS268 release (accession:
611 PRJNA13758).

612 **Principal component analysis**

613 The N2 and JU1400 normalised abundance measurements generated by Alaska, were read by
614 the readRDS() function of the R package base v4.1.1. Normalized counts for each gene in each
615 strain were generated via sleuth_to_matrix() with the “obs_norm” data and “tpm” units. PCA of
616 gene expression was performed using samples from each strain, and merged samples, via the R
617 package pcaexplorer v2.20.2 [87].

618 **Differentially expressed genes of N2 and JU1400 hosts**

619 Log2 fold change values of duplicated genes in each of the eight samples were averaged using
620 the R package dplyr v1.0.8. Genes with FDR-adjusted p-value of <0.01 were regarded as
621 significant. Significant genes expressed in at least three out of the eight samples were used for
622 hierarchical clustering via the function hclust() from the R package stats v4.1.1, then plotted using
623 R packages ggdendrogram and ggplot2 v3.3.5. Differentially upregulated genes were defined as
624 those with an FDR-adjusted p-value<0.01 and log2 fold change ≥0 (infected vs. control);
625 differentially downregulated genes were defined as those with an FDR-adjusted p-value <0.01
626 and log2 fold change ≤0 (infected vs. control).

627 **Strain-specific, pathogen-specific and strain-pathogen pair specific genes**

628 Strain-specific genes were defined as genes that are significantly upregulated or downregulated
629 in at least three out of the four JU1400 or N2 samples. Pathogen-specific genes were defined as
630 those significantly upregulated or downregulated in both JU1400 and N2 upon infection by the
631 same microsporidia species, but not observed when infected by other microsporidia species.
632 Moreover, strain-pathogen pair specific genes were defined as genes that are significantly

633 upregulated or downregulated in a particular strain-pathogen sample, but not observed in the
634 other seven strain-pathogen samples.

635 **Domain enrichment analysis**

636 We chose to look at F-box, MATH/BATH, PALS, DUF684 and DUF713 domains containing
637 genes, implicated from differentially regulated genes of *N. parisii* infected *C. elegans* in previous
638 publications [88,89]. Lists of gene names from respective gene classes were downloaded
639 separately from Wormbase (http://wormbase.org/) and the corresponding protein-coding
640 sequences were extracted from Wormbase ParaSite (https://parasite.wormbase.org/).
641 Alignments of other domains or classes were downloaded directly from Pfam
642 (http://pfam.xfam.org/) separately. After deleting duplicated sequences, protein sequences of
643 these classes of genes were converted to Stockholm format using Clustal Omega Multiple
644 Sequence Alignment tool (https://www.ebi.ac.uk/Tools/msa/clustalo/). Hmmbuild of HMMER
645 v3.3.2[90] used the Stockholm format files to build respective profile HMMs, which was then
646 searched against *C. elegans* (accession: PRJNA13758) proteome of WS268 release using
647 hmmsearch. Output genes with E-value <1e-5 were used as the gene list for the enrichment
648 analyses. In the output genes, MATH and BATH genes were combined into one list; fbxa, fbxb
649 and fbxc genes were merged into the gene list for F-box (**Supplementary Table S10**). Using the
650 R package gplots v3.1.1, the number of genes overlapping between the lists and samples were
651 computed, then plotted using R package ggplot2 v3.3.5. Genes that do not fall into any of these
652 gene classes or have any of these domains were categorised as “other”.

653 **Gene Set Enrichment Analysis**

654 The WormExp [59] dataset, which contains published expression data for *C. elegans*, was
655 downloaded from the WormExp v1.0 website (https://wormexp.zoologie.uni-kiel.de/wormexp/).
656 The overlap between published datasets of *C. elegans* exposed to different chemicals or

657 pathogens (**Supplementary Table S9**) and our samples, as well as the strain specific, pathogen-
658 specific, and strain-pathogen pair specific genes in our dataset were computed using the R
659 package gplots v3.1.1. For the statistical evaluation of the overlap, the p-values were calculated
660 using the adjusted Fisher exact test method from the program EASE, which removes one gene
661 in the set of intersected genes. Correction for multiple testing were implemented using the
662 Bonferroni method via the p.adjust() of the R package stats v4.1.1.

663 **Volcano plots**

664 Values of duplicated genes in each of the four host-microsporidia samples were averaged using
665 the R package dplyr v1.0.8. Genes with FDR<0.05 and log2 Fold Change >0 or log2 Fold Change
666 <0 were categorised as differentially upregulated or downregulated respectively. The volcano
667 plots were generated by ggplot2 v3.3.5 in R.

668 **Data and code availability**

669 All samples were deposited under NCBI BioProject PRJNA841603 and the sequence reads for
670 all samples were submitted to the NCBI Sequence Read Archive. Data from all the infection
671 experiments is in **Supplementary Data S1**. PhenoMIP analysis scripts can be found at
672 https://github.com/camok/PhenoMIP.

673

674 **Figures**

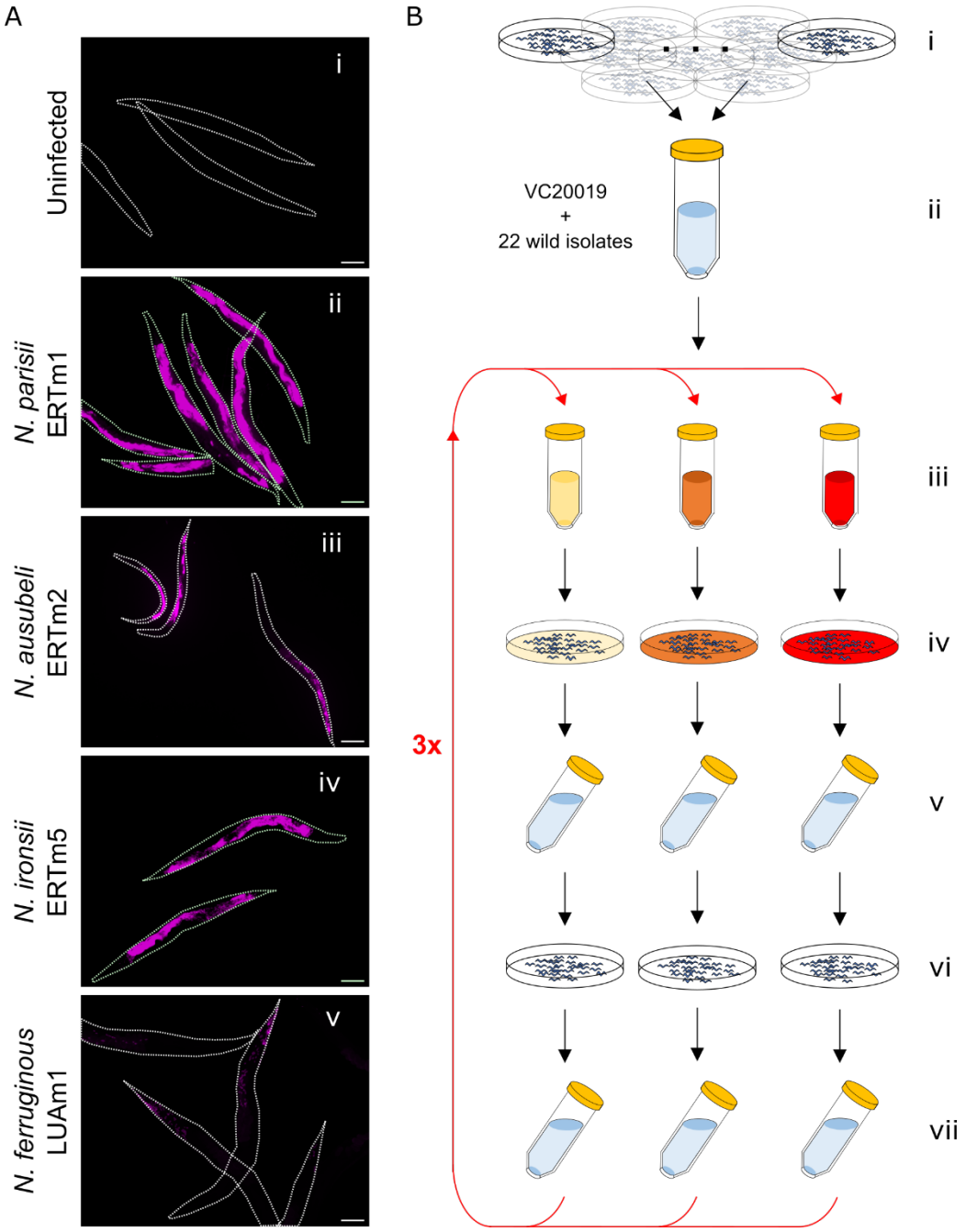

675

676 **Figure 1. A PhenoMIP high-throughput screen to identify wild strains that are either**
677 **resistant or susceptible to microsporidia infection.** (A) N2 L1 animals that were uninfected (i)
678 or exposed to either 3.5 million *N. parisii*, *N. ironsii*, or *N. ausubeli* spores or 1.25 million *N.*
679 *ferruginous* spores for 72 hours, were fixed and stained with the following 18S FISHs probes (i,

680 ii, iv; MicroB-CAL Fluor Red 610, iii; Microsp1A-FAM and v; a combination of three Fluor Red 610
681 probes described in the Methods). Scale bars, 100 μm. (B) PhenoMIP screening protocol for
682 microsporidia requires that separate unstarved populations for each of 22 wild isolate strains as
683 well as VC20019 (lab reference-derived strain) be sodium hyplochlorite-synchronized (i) before
684 pooling in equimolar amounts (ii) and infecting (iii) with different microsporidia species at doses
685 that can impose fitness challenges to the lab reference strain. Populations are grown for 72 hours
686 post-infection (iv) before sodium hypochlorite-synchronizing (v) and grow free of infection for an
687 additional 72 hours (vi). Uninfected populations are harvested, subsampled for genomic DNA,
688 and sodium hypochlorite-synchronized (vii) before repeating the infection and rest phases for an
689 additional three rounds.

690

691

692

693

694

695

696

697

698

699

700

701

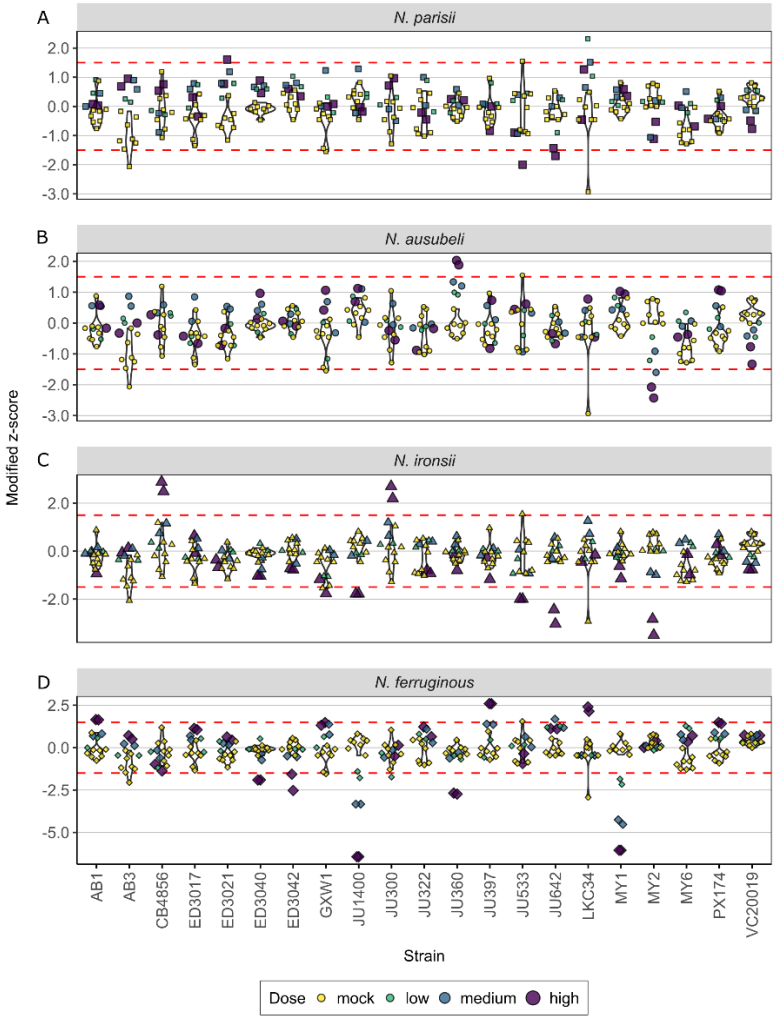

Figure 2. Analysis of PhenoMIP mean fold-change rate identifies candidate nematode/microsporidia interactions. Violin plots of 20 wild isolates and lab reference-derived control strain VC20019 showing modified z-scores of mean fold-change rate (FCR) per generation derived from the eight mock-infection replicates. Overlayed are the six infection replicates for each of *N. parisii* (A), *N. ausubeli* (B), *N. ironsii* (C), and *N. ferruginous* (D). Replicates are coloured by mock infection (yellow), low dose (green), medium dose (blue), and high dose (purple) with increasing point size associated with increasing dose. Dotted lines represent the z-score candidate threshold of ±1.5. The strains CB4854 and JU312 were excluded from analysis due to low initial population abundance.

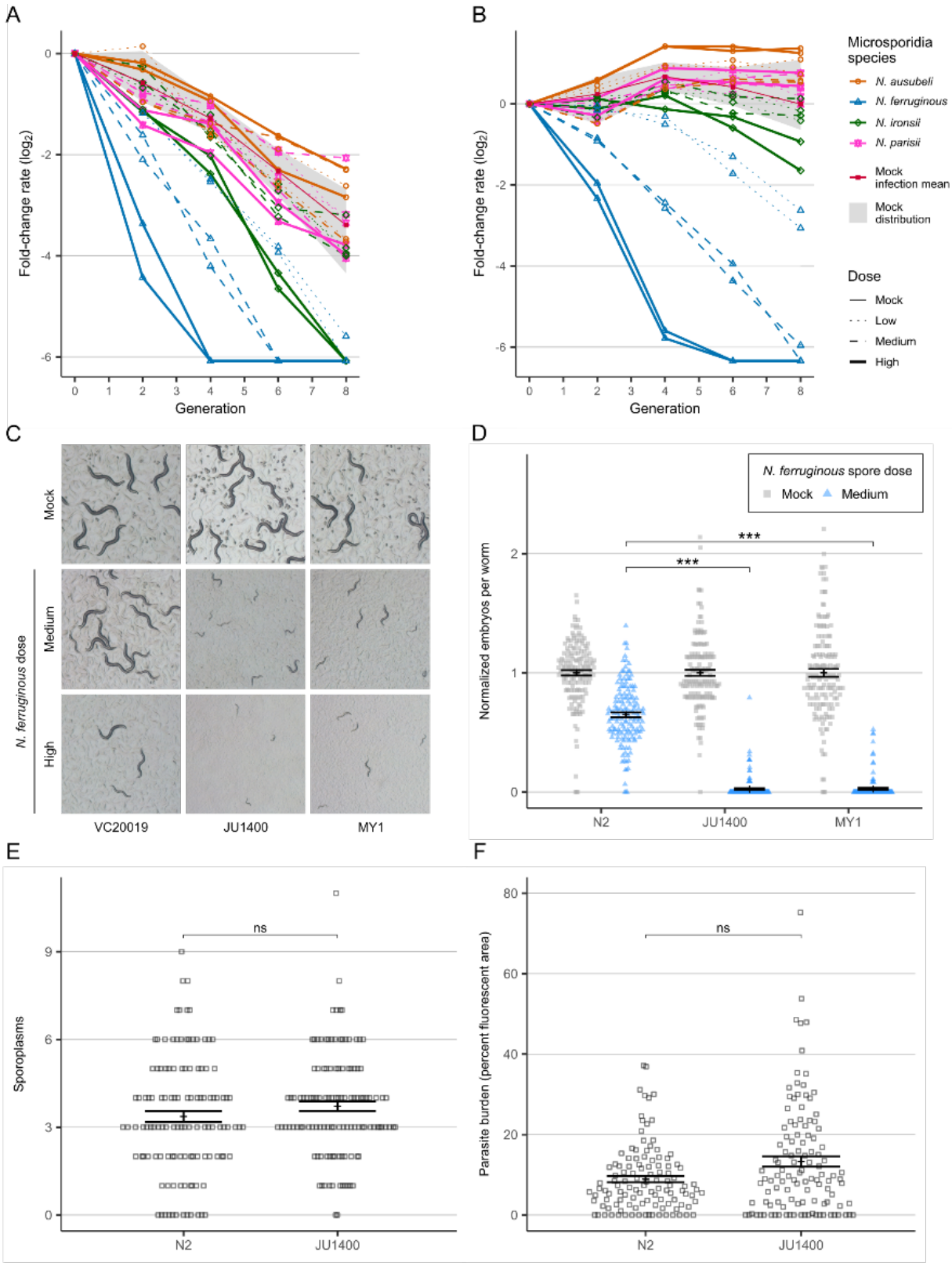
A
Fold-change rate (log2)
Generation
B
Microsporidia species
N. ausubeli
N. ferruginous
N. ironsii
N. parisii
Mock infection mean
Mock distribution
Dose
Mock
Low
Medium
High
C
Mock
N. ferruginous dose
Medium
High
VC20019
JU1400
MY1
D
N. ferruginous spore dose
Mock
Medium
Normalized embryos per worm
***
N2
JU1400
MY1
E
Sporoplasms
ns
N2
JU1400
F
Parasite burden (percent fluorescent area)
ns
N2
JU1400

712

713 **Figure 3. JU1400 lacks tolerance to N*. ferruginous* infection.** (A-B) Line graph of fold change
714 across multiple time points and conditions for JU1400 (A) and MY1 (B). Microsporidia strains are
715 denoted by point shape and doses of microsporidia are denoted by line type. The eight uninfected
716 control replicates are bounded within the greyed area and the mean of the uninfected control is
717 denoted by a solid red line. (C-D) Strains were infected for 72 hours with *N. ferruginous*. (C)
718 Dissecting microscope images of live animals growing on plates. (D) Dotplot of normalized
719 embryo counts of animals fixed and stained with DY96 with mean and SEM bars. Data is
720 combined from three biological replicates with n={41,50} worms per replicate sample. (E-F) N2
721 and JU1400 animals were infected for three hours with 1.25 million spores of *N. ferruginous* before
722 washing away uneaten spores from each population. (E) Dotplot of sporoplasms counted in N2
723 and JU1400 animals fixed immediately after infection. Data is combined from three biological
724 replicates with n=40 worms per replicate sample. (F) Barplot with SEM bars depicting mean
725 parasite burden as a function of percent fluorescent area per animal by FISH staining in N2 and
726 JU1400 populations fixed at 72 hpi. Data is combined from three biological replicates with n={29,
727 53} worms per replicate sample. p-values were determined by two-way ANOVA with Tukey post-
728 hoc. Significance was defined as $p \leq 0.001$ (***) and not significant as $p > 0.05$ (ns).

729

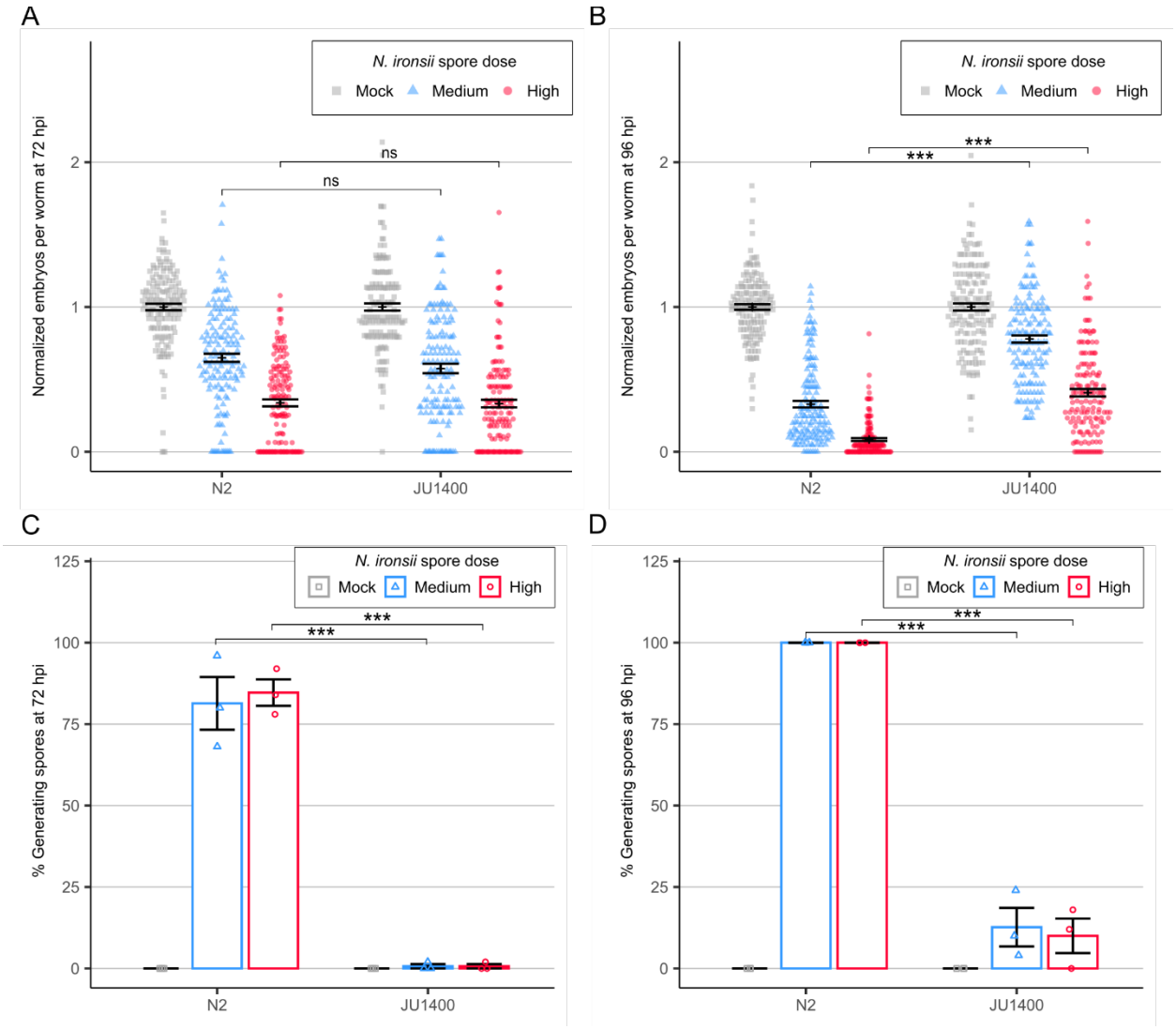

730

731 **Figure 4. JU1400 is resistant to *Nematocida ironsii* infection.** (A-D) N2 and JU1400 were
732 infected with *N. ironsii* for 72 hours (A and C) or 96 hours (B and D), fixed and stained with DY96.
733 (A-B) Dotplots of normalized embryo counts of animals fixed and stained with DY96 with mean
734 and SEM bars. Data is combined from three biological replicates with n={47,50} worms per
735 replicate sample. (C-D) Barplot with SEM bars of percent population with new spore formation
736 from three combined replicate experiments. p-values were determined by two-way ANOVA with
737 Tukey post-hoc. Significance was defined as $p \leq 0.001$ (***) and not significant as $p > 0.05$ (ns).

738

739

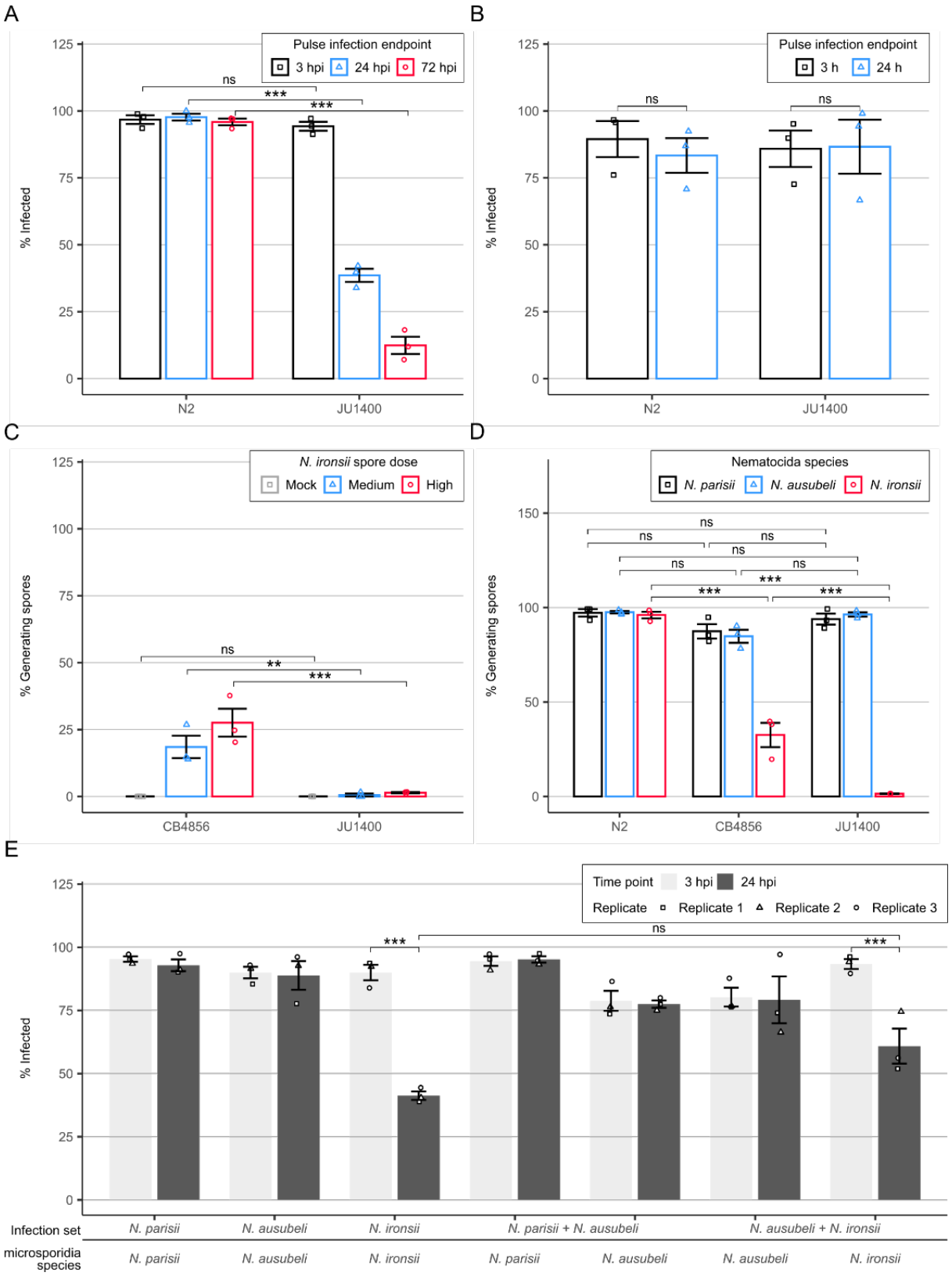
A
Pulse infection endpoint
3 hpi
24 hpi
72 hpi
% Infected
N2
JU1400
B
Pulse infection endpoint
3 h
24 h
% Infected
N2
JU1400
C
N. ironsii spore dose
Mock
Medium
High
% Generating spores
CB4856
JU1400
D
Nematocida species
N. parisii
N. ausubeli
N. ironsii
% Generating spores
N2
CB4856
JU1400
E
Time point
3 hpi
24 hpi
Replicate
Replicate 1
Replicate 2
Replicate 3
% Infected
Infection set
N. parisii
N. ausubeli
N. ironsii
N. parisii + N. ausubeli
N. ausubeli + N. ironsii
microsporidia species
N. parisii
N. ausubeli
N. ironsii
N. parisii
N. ausubeli
N. ausubeli
N. ironsii

741 **Figure 5. JU1400 specifically clears *N. ironsii* infection at the earliest larval stage.** (A-B) N2
742 and JU1400 animals were pulse infected for 3 hours with *N. ironsii* before washing away excess
743 spores. Animals were pulse infected at either the L1 stage and fixed at 3-, 24-, and 72 hpi (A) or
744 animals were pulse infected at the L4 stage before fixing at 3- and 24 hpi (B). Samples were then
745 stained with an *N. parisii* 18S RNA FISH probe and animals containing either sporoplasms or
746 meronts were counted as infected. Barplot with SEM bars show percent of animals infected per
747 replicate from three biological replicates with n=20 worms per replicate. (C-D) N2, JU1400, and
748 CB4856 were infected at the L1 stage with either *N. parisii*, *N. ausubel*, or *N. ironsii* for 72 hours
749 and then fixed and stained with DY96. Barplot with SEM bars show percent of animals generating
750 spores per replicate from three biological replicates with n=20 worms per replicate. (E) JU1400
751 animals were pulse infected for 3 hours with *N. parisii*, *N. ausubeli*, *N. ironsii, N. parisii* + *N.*
752 *ausubeli, or N. ausubeli* + *N. ironsii* before washing away excess spores. Animals were either
753 fixed immediately at 3 hpi or at 24 hpi. Samples were then stained with species-specific 18S rRNA
754 FISH probes and animals containing either sporoplasms or meronts were counted as infected.
755 Barplot with SEM bars show percent of animals infected per replicate from three biological
756 replicates with n={78, 147} worms per replicate. P-values were determined by two-way ANOVA
757 with Tukey post-hoc. Significance was defined as $p \leq 0.01$ (**), $p \leq 0.001$ (***) and not significant
758 as $p > 0.05$ (ns).

759

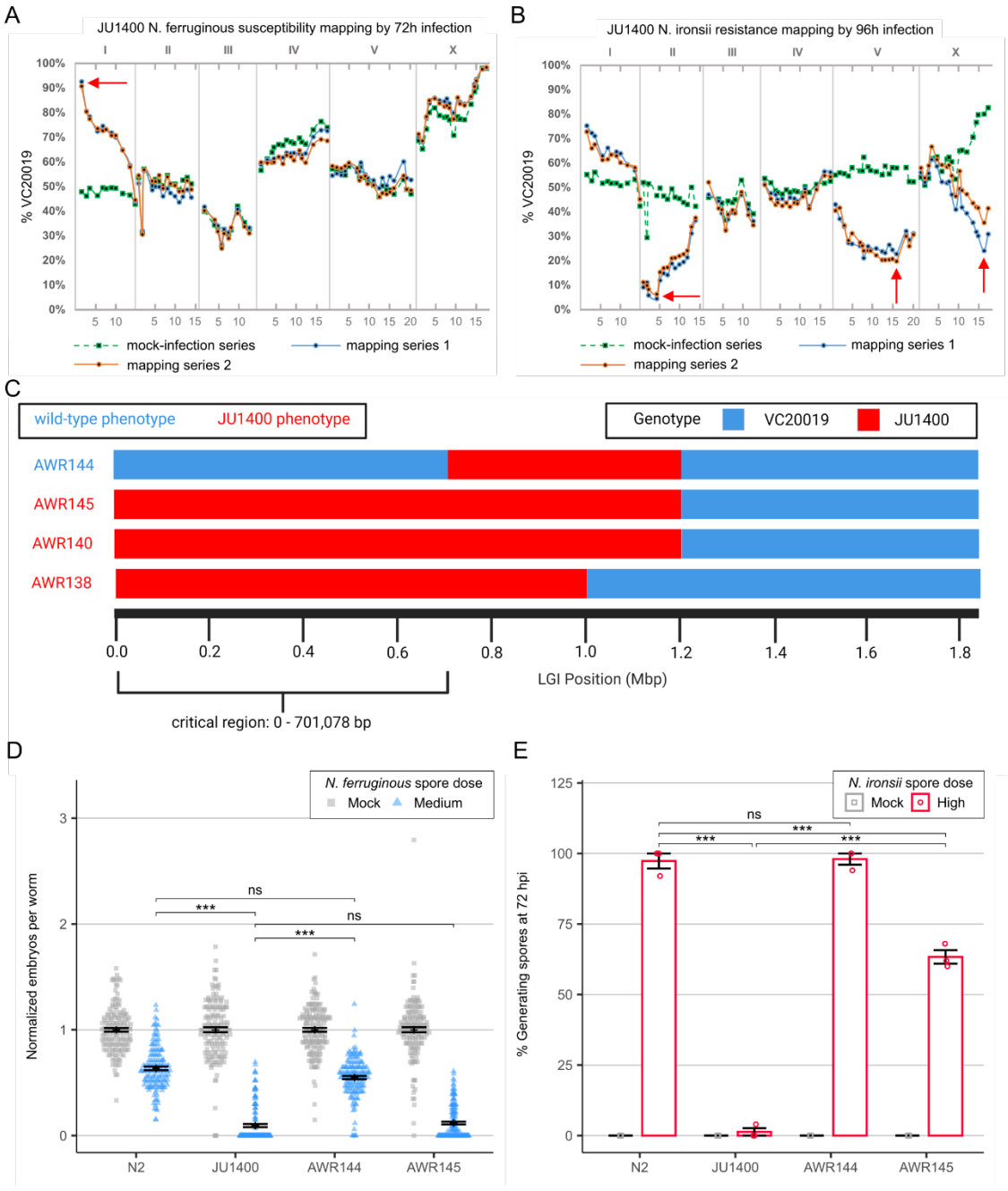

Figure 6. Genetic mapping of JU1400 host-response phenotypes identifies distinct loci. Genetic mapping of JU1400 susceptibility to *N. ferruginous* (A) and JU1400 resistance to *N. ironsii* (B) was performed with MIP-MAP using the AWR133 mapping strain. Green square-points and dotted lines represent a mock-infection replicate with the solid blue and orange lines representing two biological replicates exposed to specific infection conditions. Red arrows indicate candidate

766 regions of interest based on the expected genome fixation direction during phenotype selection.
767 (C) Whole-genome sequencing haplotype map of chromosome I near-isogenic lines (NILs)
768 generated from crosses between JU1400 and AWR133. Regions of chromosome I for specific
769 NILs are coloured by their inferred haplotype. Strain names are indicated to the left of each with
770 AWR138, AWR140, and AWR145 sharing a susceptibility phenotype (Red text) while AWR144 is
771 not susceptible (Blue text) to *N. ferruginous* infection. (D) N2, JU1400, AWR144, and AWR145
772 L1 stage animals were infected with *N. ferruginous* before being fixed at 72hpi and stained with
773 DY96 to visualize embryos. Dotplot of normalized embryo counts of with mean and SEM bars.
774 Data is combined from three biological replicates with n=50 worms per replicate sample. (E) N2,
775 JU1400, AWR144, and AWR145 L1 stage animals were infected with *N. ironsii* before being fixed
776 at 72hpi and stained with DY96 to visualize mature spores. Barplot with SEM bars show percent
777 of animals generating new spores per replicate from three biological replicates with n=50 worms
778 per replicate. p-values were determined by two-way ANOVA with Tukey post-hoc. Significance
779 was defined as $p \leq 0.001$ (***) and not significant as $p > 0.05$ (ns).

780

781

782

783

784

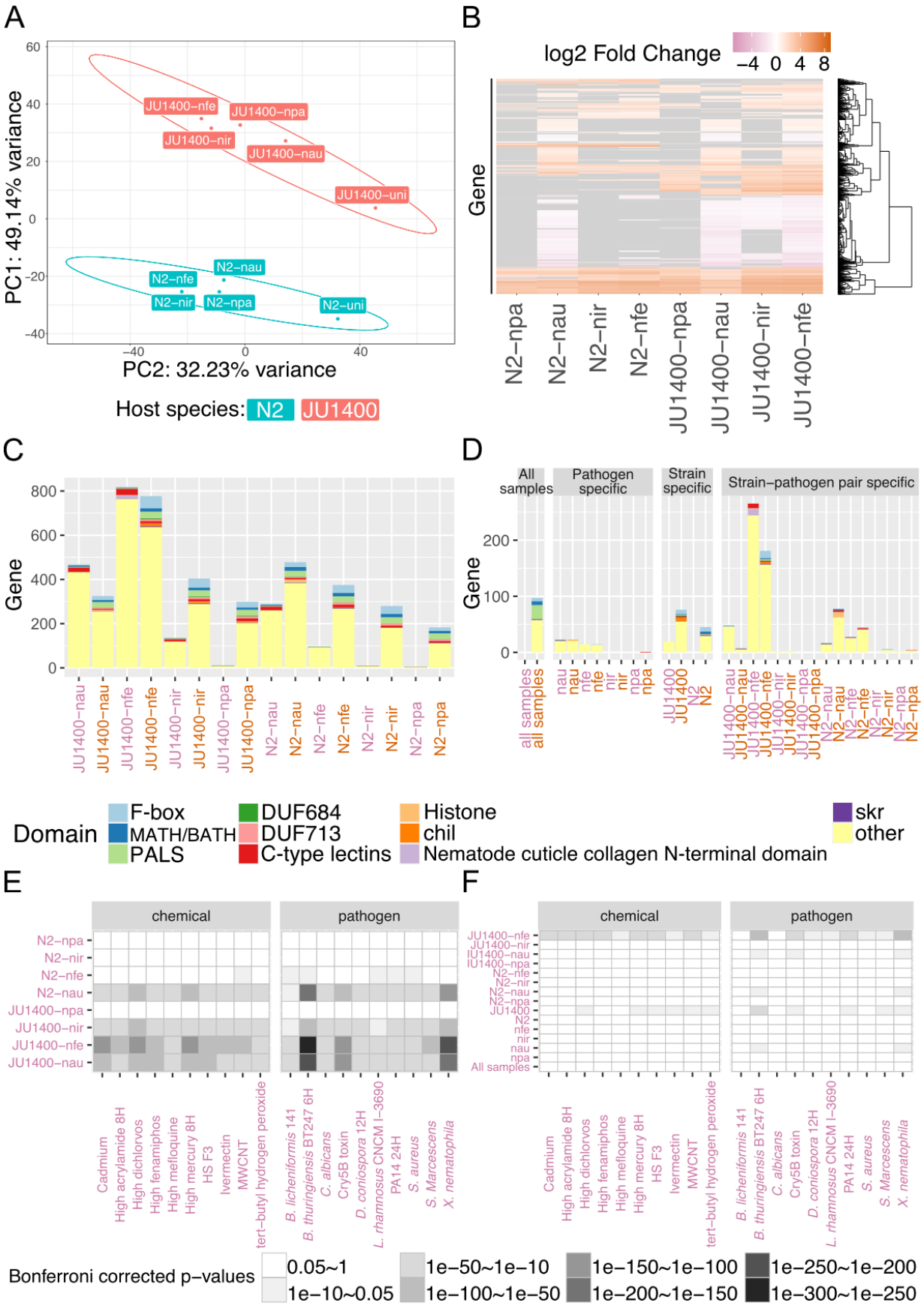
A
PC1: 49.14% variance
PC2: 32.23% variance
JU1400−nfe
JU1400−npa
JU1400−nir
JU1400−nau
JU1400−uni
N2−nau
N2−nfe
N2−nir
N2−npa
N2−uni
Host species: N2 JU1400
B
log2 Fold Change
−4 0 4 8
Gene
N2−npa
N2−nau
N2−nir
N2−nfe
JU1400−npa
JU1400−nau
JU1400−nir
JU1400−nfe
C
Gene
D
All samples
Pathogen specific
Strain specific
Strain−pathogen pair specific
Domain
F-box
MATH/BATH
PALS
DUF684
DUF713
C-type lectins
Histone
chil
Nematode cuticle collagen N-terminal domain
skr
other
E
chemical
pathogen
Cadmium
High acrylamide 8H
High dichlorvos
High fenamiphos
High mefloquine
High mercury 8H
HS F3
Ivermectin
MWCNT
tert−butyl hydrogen peroxide
B. licheniformis 141
B. thuringiensis BT247 6H
C. albicans
Cry5B toxin
D. coniospora 12H
L. rhamnosus CNCM I−3690
PA14 24H
S. aureus
S. Marcescens
X. nematophila
F
Bonferroni corrected p−values
0.05~1
1e−10~0.05
1e−50~1e−10
1e−100~1e−50
1e−150~1e−100
1e−200~1e−150
1e−250~1e−200
1e−300~1e−250

785

786 **Figure 7. RNA-seq analysis of N2 and JU1400 infected with four species of microsporidia.**
787 N2 and JU1400 animals were infected with one of four species of microsporidia (see Methods for
788 doses) for 48 hours and RNA was extracted and sequenced. (A) Principal component analysis of
789 uninfected and infected N2 and JU1400 samples. Circles represent confidence ellipses around
790 each strain at 95% confidence interval. (B) Heatmap of transcriptional profiles of differentially
791 regulated genes in N2 and JU1400 samples. Rows represent gene clustered hierarchically. Scale
792 is of differential regulation of infected compared to uninfected samples. Grey tile indicates that
793 the gene is not expressed in the sample. (C-D) Domain enrichment analysis of significantly
794 upregulated and downregulated genes in each sample (C) and of specific gene sets (strain,
795 pathogen, and strain-pathogen pair) (D). (E-F) Overlap between published datasets of
796 differentially expressed *C. elegans* genes upon exposure to chemicals or bacterial infection and
797 downregulated genes from each sample (E) or from strain specific, pathogen specific, strain-
798 pathogen pair specific gene sets. (A-F) uni (uninfected), npa (*N. parisii)*, nau (*N. ausubeli*), nir (*N.*
799 *ironsii),* and nfe (*N. ferruginous)*. Upregulated samples are represented with orange text;
800 downregulated samples are represented with pink text.

801

802

803

804

805

806

807

808

809 **Supplementary material**

810 **Figure S1. Geographical locations of *C. elegans* and microsporidia used in this study.**

811 **Figure S2. The Hawaiian (CB4856) strain shows resistance to infection by high-dose *N.***
812 ***ironsii*.**

813 **Figure S3. Single-strain testing of PhenoMIP interaction candidates with *N. ferruginous***
814 **infection.**

815 **Figure S4. Single-strain testing of PhenoMIP interaction candidates with *N. ironsii***
816 **infection.**

817 **Figure S5. Single-strain testing of PhenoMIP interaction candidates with *N. ausubeli***
818 **infection replicates.**

819 **Figure S6. JU1400 and MY1 share similar response phenotypes to infection by *N.***
820 ***ferruginous*.**

821 **Figure S7. JU1400 and N2 display similar levels of *N. ferruginous* infection.**

822 **Figure S8. JU1400 displays a similar response to *N. ferruginous* strains and sensitivity to**
823 ***N. cider*.**

824 **Figure S9. JU1400 is resistant to infection by *N. ironsii*.**

825 **Figure S10. JU1400, but not N2, can specifically eliminate *N. ironsii* infection.**

826 **Figure S11. Genetic mapping of CB4856 resistance to *N. ironsii.***

827 **Figure S12. Genetic mapping of interaction phenotypes of JU1400 to *N. ironsii* and MY1 to**
828 ***N. ferruginous* using 72-hour selections.**

829 **Figure S13. JU1400 and MY1 susceptibility to *N. ferruginous* is recessive and MY1 is less**
830 **resistant than JU1400 to ERTm5.**

831 **Figure S14. Generation of near-isogenic lines carrying the chromosome I region that is**
832 **responsible for susceptibility to *N. ferruginous*.**

833 **Figure S15. Microsporidia mRNA reads per sample demonstrates JU1400 resistance to *N.***
834 ***ironsii*.**

835 **Figure S16. Principal component analysis of N2 and JU1400 samples.**

836 **Figure S17. Comparison of correlation between N2 and JU1400 strains after infection with**
837 **different microsporidia species.**

838 **Figure S18. Volcano plots of differentially regulated genes.**

839 **Figure S19. Overlap between the significant upregulated genes upon microsporidia**
840 **infection and differentially expressed datasets of *C. elegans* genes upon exposure to**
841 **chemicals or bacterial infection.**

842 **Table S1. Microsporidia species information.**

843 **Table S2. PhenoMIP microsporidia infection doses.**

844 **Table S3. Wild isolate mapping microsporidia infection doses.**

845 **Table S4. NIL strain chromosome I region composition.**

846 **Table S5. Microsporidia gene FPKM values in N2 and JU1400.**

847 **Table S6: Normalized *C. elegans* gene counts for all RNA-seq replicates from this study.**

848 **Table S7: Results of *C. elegans* differential expression analyses for all RNA-seq**
849 **comparisons performed in this study.**

850 **Table S8. Gene classes and domains used for enrichment analyses.**

851 **Table S9. Published data sets from WormExp used in this study.**

852 **Table S10. List of gene set overlaps to other data sets.**

853 **Data S1. Data of all infection experiments.**

854

855

856

857

858

859

860

861

A

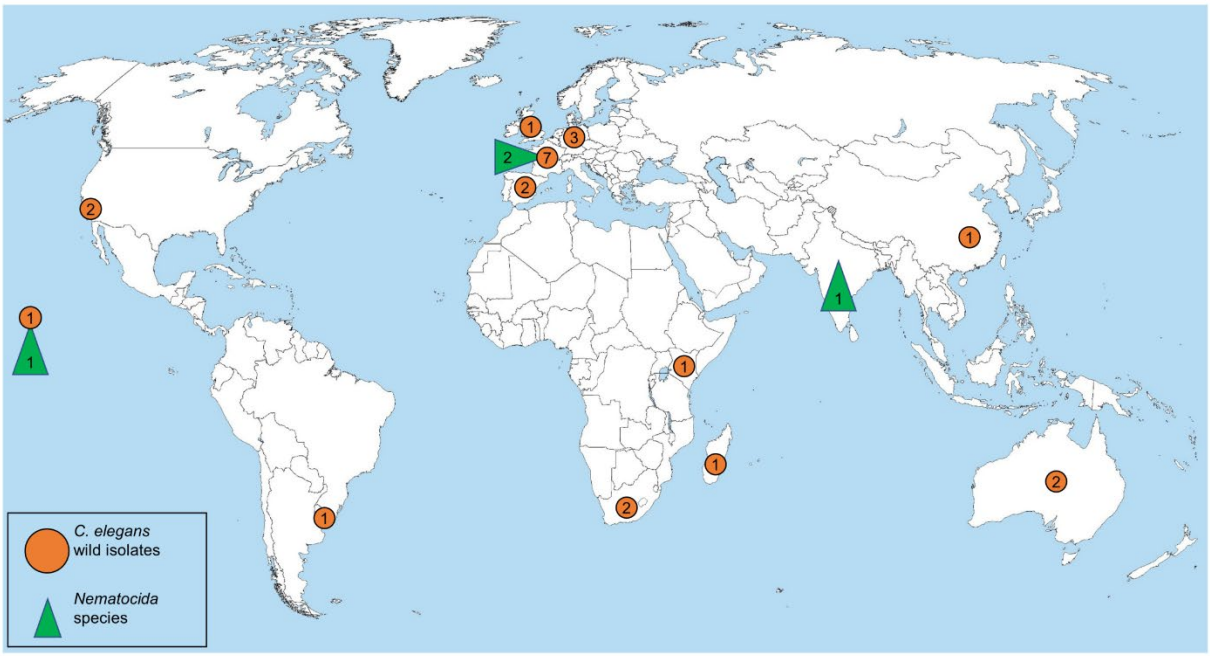

862

863 **Figure S1. Geographical locations of *C. elegans* and microsporidia used in this study.** (A)

864 World map highlighting the locations where the *C. elegans* wild isolate strains (orange circles)

865 and *Nematocida* species (green triangles) used in this study were originally isolated.

870

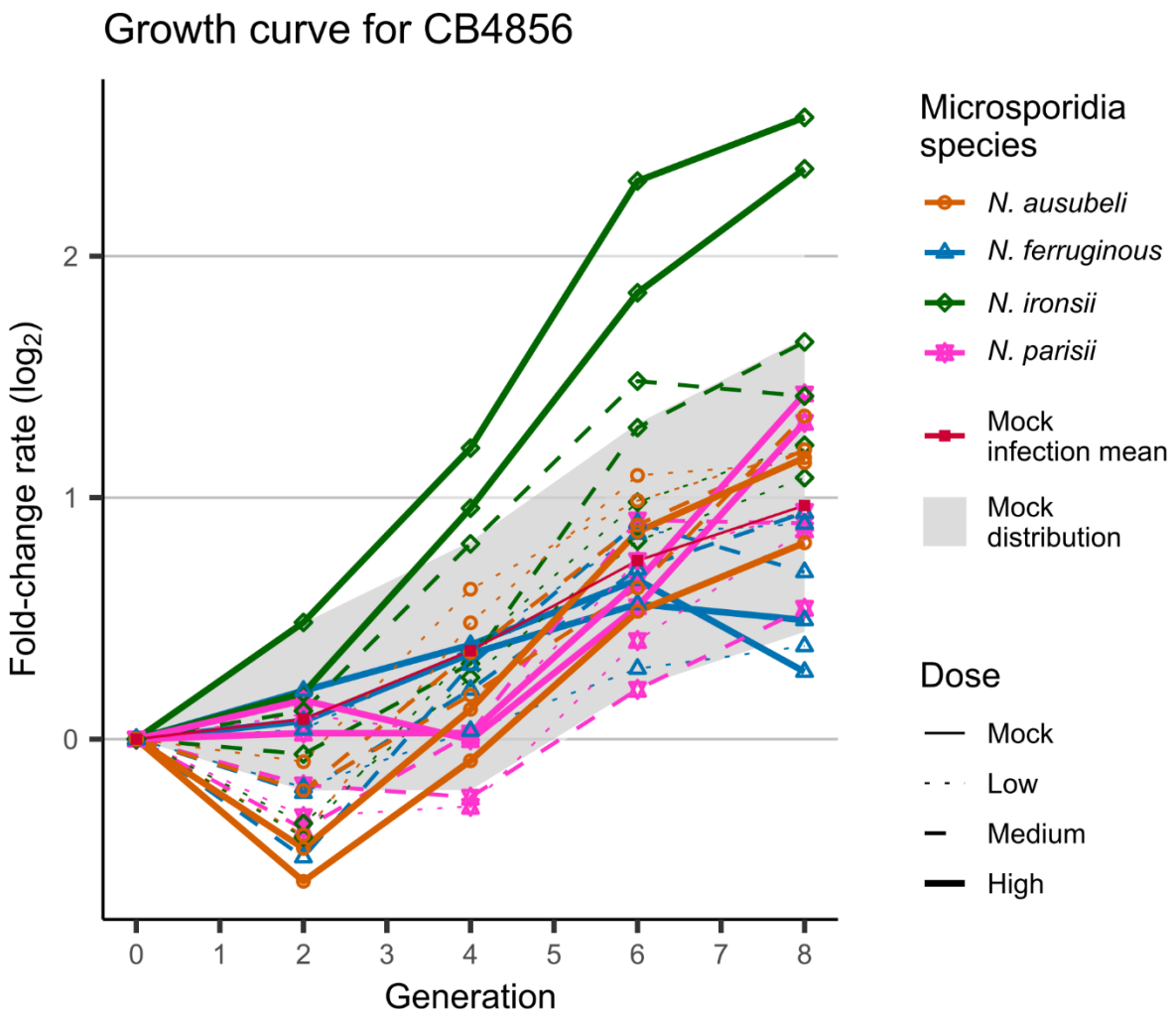

871

872 **Figure S2. The Hawaiian (CB4856) strain shows resistance to infection by high-dose *N.***
873 ***ironsii*.** Line graph of fold change across multiple time points and conditions for CB4856
874 demonstrates potential fitness increase relative to mock-infection conditions when infected with
875 *N. ironsii*. Microsporidia strains are denoted by point shape and doses of microsporidia are
876 denoted by line type. The eight uninfected control replicates are bounded within the greyed area
877 with the mean of the uninfected controls denoted by a solid red line.

878

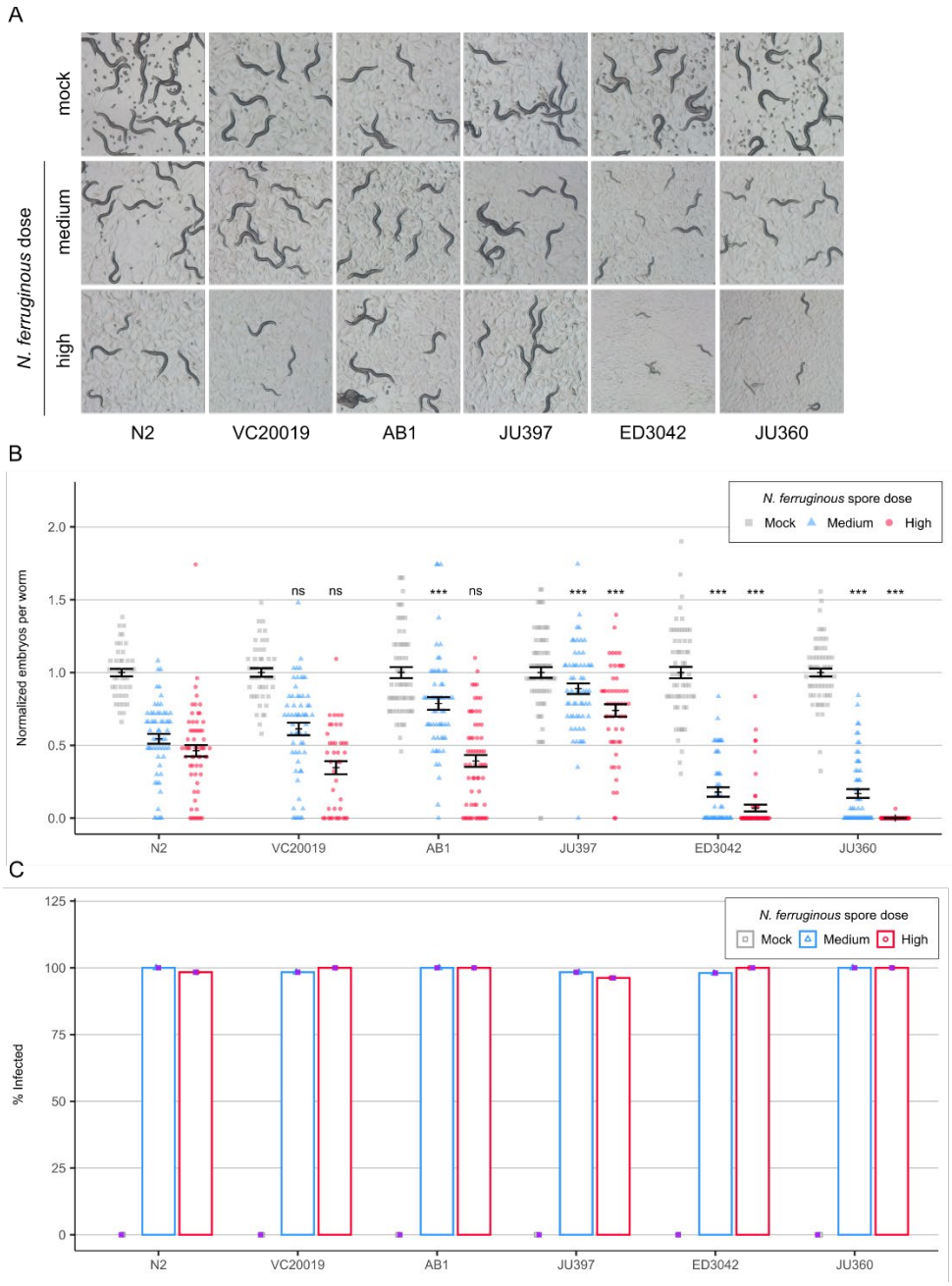

Figure S3. Figure S3. Single-strain testing of PhenoMIP interaction candidates with *N. ferruginous* infection. (A-C) Strains of *C. elegans* were infected with medium and high doses of *N. ferruginous* for 72 hours, imaged, fixed, and stained with DY96 and a *N. ferruginous* 18S rRNA FISH probe. (A) images of N2 and VC20019 controls versus AB1, JU397, ED3042, and JU360 at 72 hpi. (B) Dotplot with mean and SEM bars of normalized embryo counts from infected populations with a minimum of n={41,70} worms per sample. (C) Barplot depicting the percent of

886 animals with detectable meront staining. p-values denote comparison to N2 controls and were
887 determined by two-way ANOVA with Tukey post-hoc. Significance was defined as $p \leq 0.001$ (***)
888 and not significant as $p > 0.05$ (ns).

889

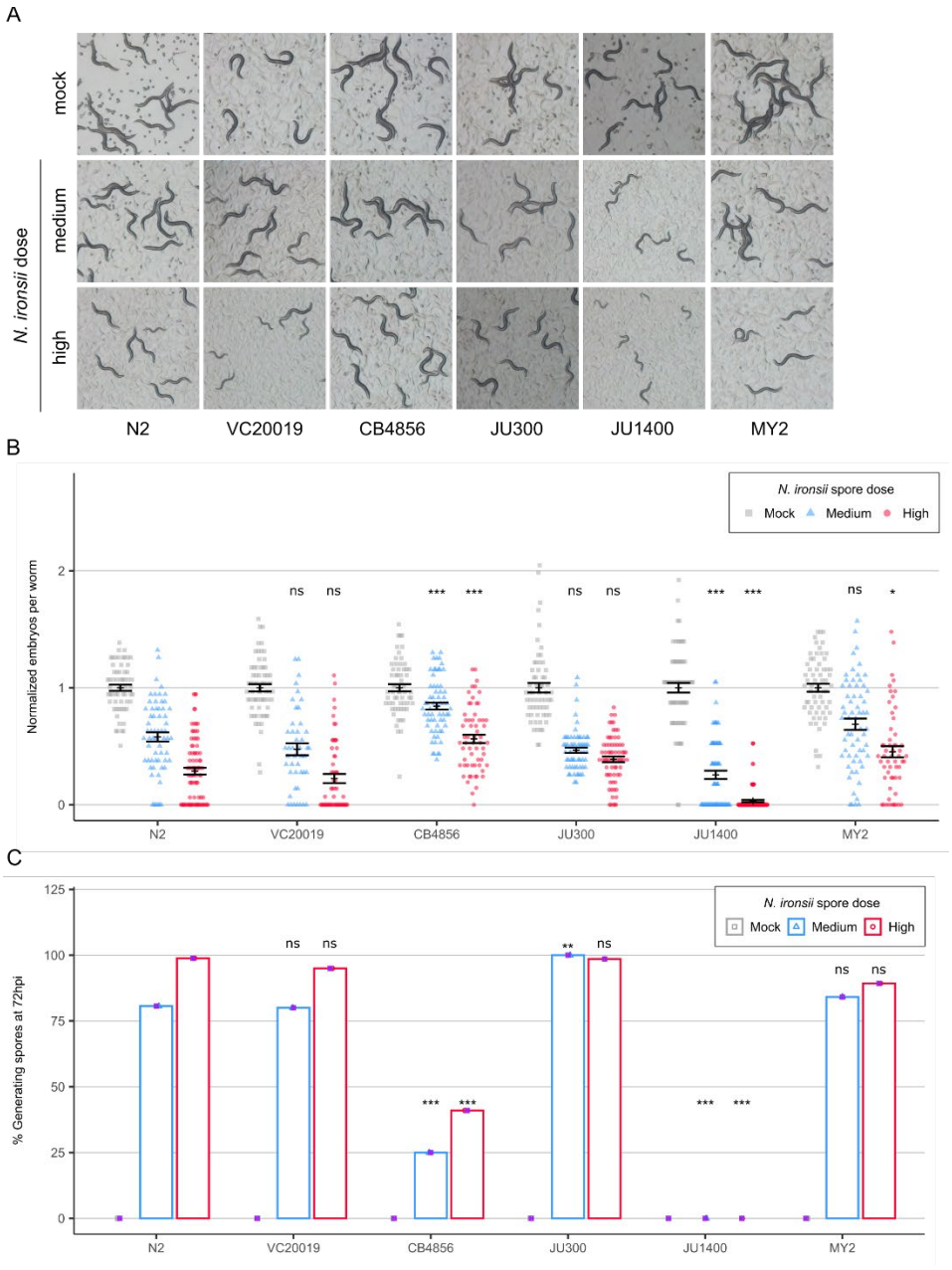

890

891 **Figure S4. Single-strain testing of PhenoMIP interaction candidates with *N. ironsii***
892 **infection.** (A-C) Strains of *C. elegans* were infected with medium and high doses of *N. ironsii* for
893 72 hours, imaged, fixed, and stained with DY96. (A) images of N2 and VC20019 controls versus
894 CB4856, JU300, JU1400, and MY2 at 72 hpi. (B) Dotplot with mean and SEM bars of normalized
895 embryo counts from infected populations with a minimum of n={45,115} worms per sample. (C)
896 Barplot depicting the percent of animals with newly generated spores. p-values denote

897 comparison to N2 controls and were determined by two-way ANOVA with Tukey post-hoc.
898 Significance was defined as $p \leq 0.001$ (***), $p \leq 0.01$ (**), $p \leq 0.05$ (*) and not significant as $p >$
899 0.05 (ns).

900

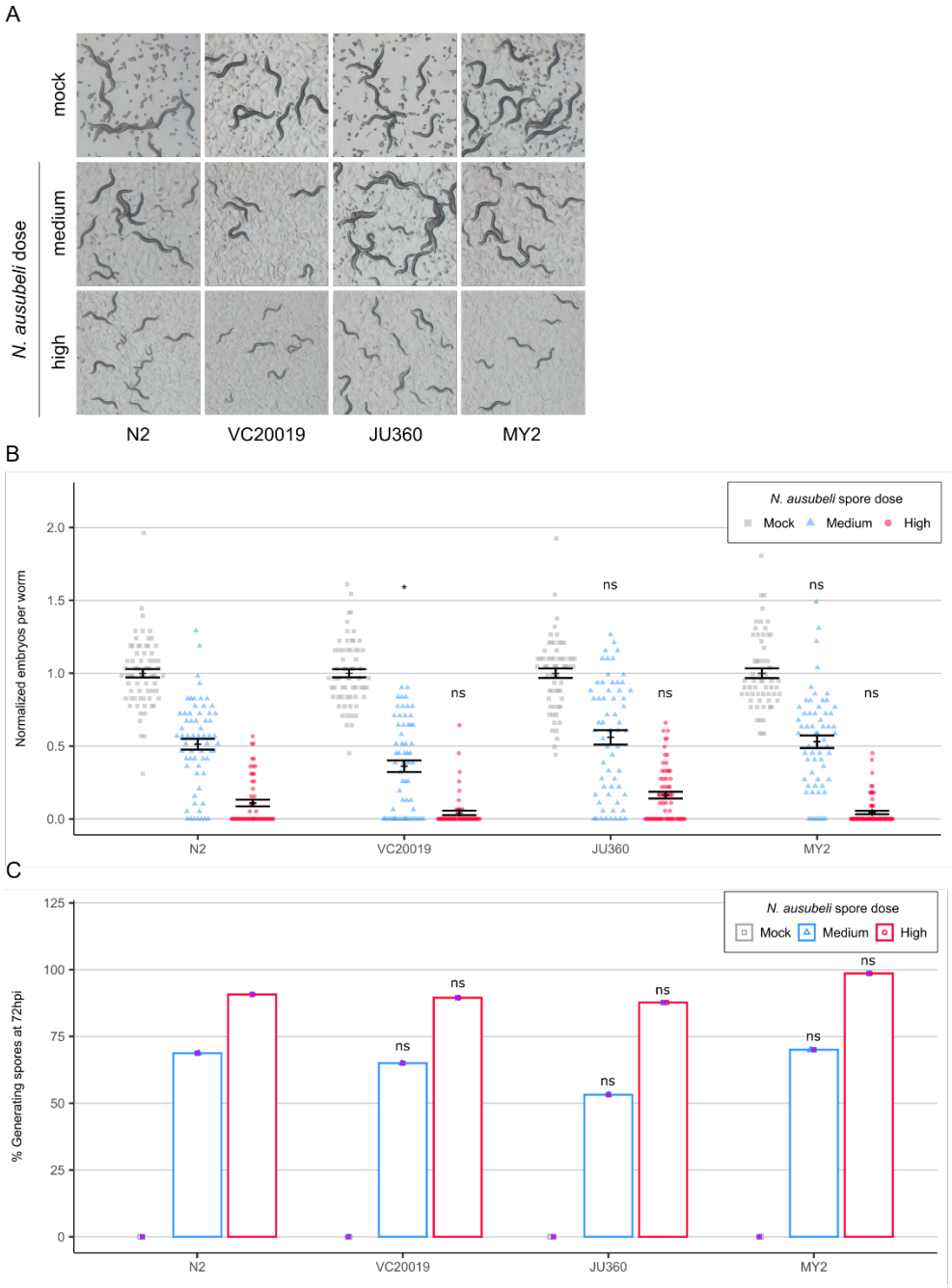

Figure S5. Single-strain testing of PhenoMIP interaction candidates with *N. ausubeli* infection. (A-C) Strains of *C. elegans* were infected with medium and high doses of *N. ausubeli* for 72 hours, imaged, fixed, and stained with DY96. (A) images of N2 and VC20019 controls versus JU360 and MY2 at 72 hpi. (B) Dotplot with mean and SEM bars of normalized embryo counts from infected populations with a minimum of n={54,71} worms per sample. (C) Barplot

907 depicting the percent of animals with newly generated spores. p-values denote comparison to N2
908 controls and were determined by two-way ANOVA with Tukey post-hoc. Significance was defined
909 as $p \leq 0.05$ (*) and not significant as $p > 0.05$ (ns).

910

911

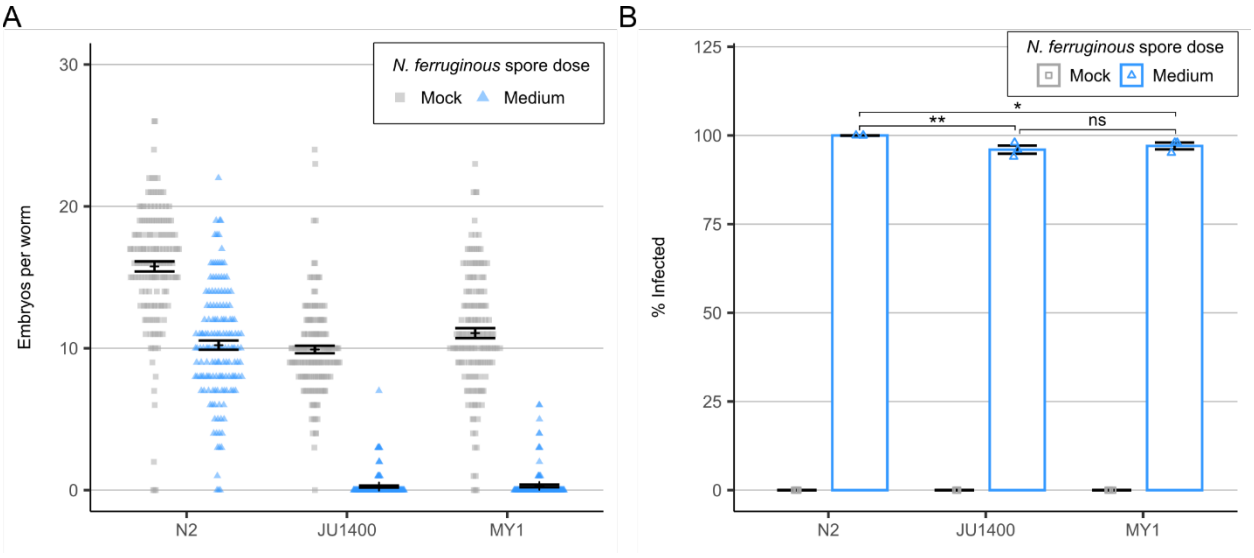

912

913 **Figure S6. JU1400 and MY1 share similar response phenotypes to infection by *N.***
914 ***ferruginous*.** JU1400, MY1 and N2 L1s were infected with a medium dose of *N. ferruginous* for
915 72 hours, fixed, and stained with *N. ferruginous* 18S rRNA FISH probes and DY96. (A) Dotplot
916 with mean and SEM bars of embryo counts from infected populations with a minimum of n={41,50}
917 worms per sample. (B) Barplot with SEM bars depicting the percent of animals with visible
918 meronts by FISH staining. p-values denote comparison to N2 controls and were determined by
919 two-way ANOVA with Tukey post-hoc. Significance was defined as $p \leq 0.01$ (**), $p \leq 0.05$ (*) and
920 not significant as $p > 0.05$ (ns).

921

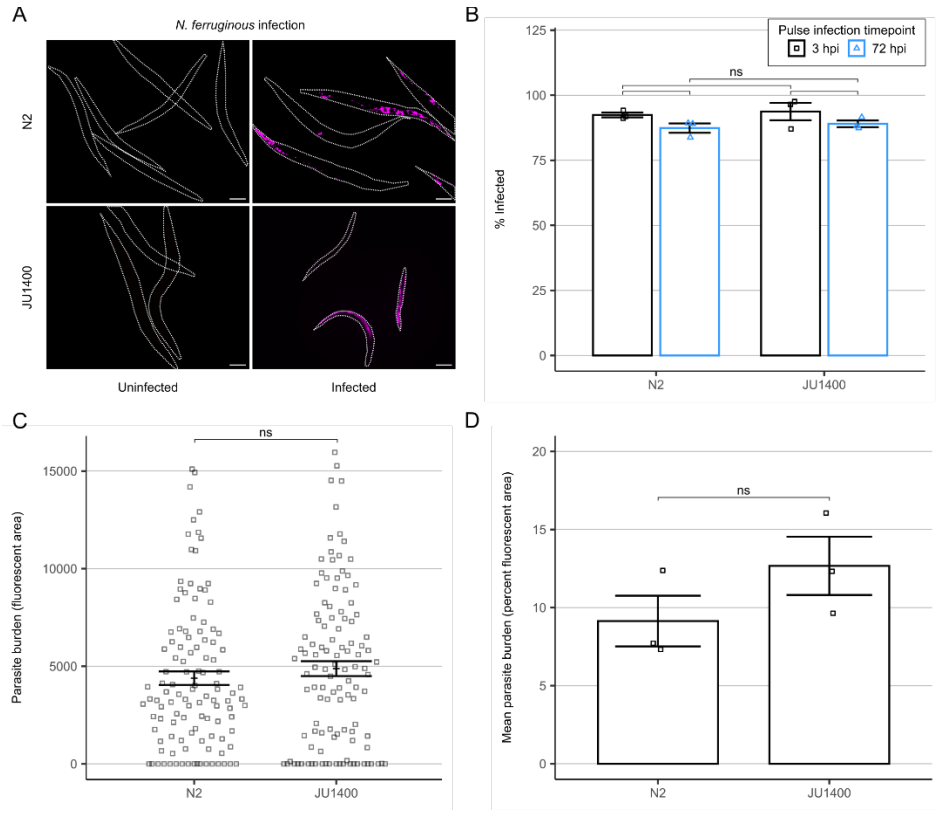

Figure S7. JU1400 and N2 display similar levels of *N. ferruginous* infection. (A-D) JU1400 and N2 L1s were infected with 1.25 million spores of *N. ferruginous* for 3 h, washed to remove spores, and replated for an additional 69 h. Animals were fixed at 3 hpi and 72 hpi and stained with *N. ferruginous* 18S rRNA FISH probes. (A) Representative images of infected animals at 72 hpi. Scale bars are 100 µm. (B) Barplot with SEM bars depicting the percent of animals displaying either sporoplasm (3 hpi) or meronts (72 hpi) by FISH staining. (C) Dotplot with mean and SEM bars of parasite burden by area in infected populations with a minimum of n={41,50} worms per sample. (D) Barplot with SEM bars depicting mean parasite burden as a function of percent fluorescent area per animal by FISH staining. Data in (C, D) is combined from three biological replicates with n=40 worms per replicate sample. p-values denote comparison to N2 or JU1400 controls and were determined by two-way ANOVA with Tukey post-hoc. Not significant was defined as $p > 0.05$ (ns).

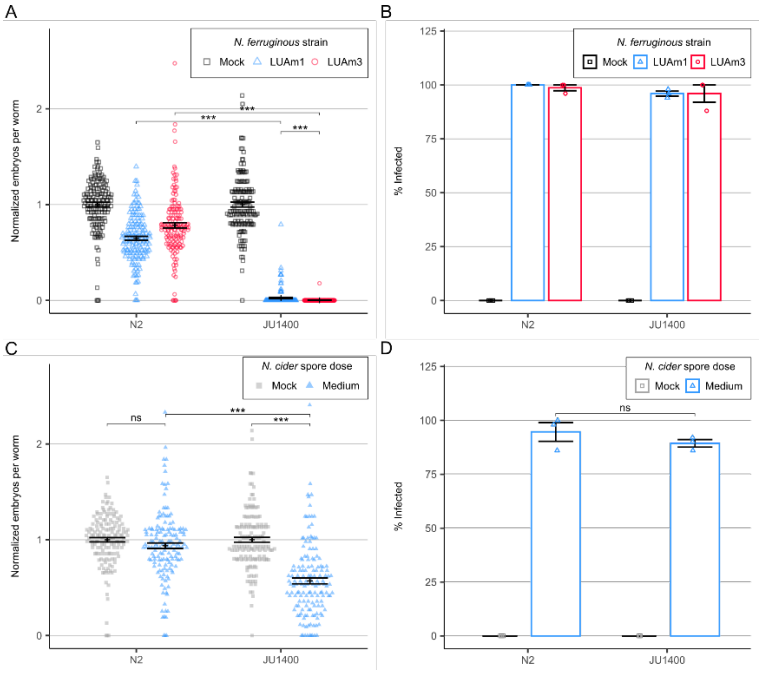

936

937 **Figure S8. JU1400 displays a similar response to *N. ferruginous* strains and sensitivity to**
938 ***N. cider*.** (A-D) N2 and JU1400 L1 stage animals were infected with medium doses of *N.*
939 *ferruginous* strain LUAm1 or LUAm3 (A-B) or a medium dose of *N. cider* (C-D) for 72 hours, fixed,
940 and stained with DY96 and a 18S rRNA FISH probe. (A, C) Dotplot of normalized embryo counts
941 of animals with mean and SEM bars. (B, D) Barplot with SEM bars of percent population with
942 meronts visible . Data are combined from three biological replicates with n=50 worms per
943 replicate. p-values were determined by two-way ANOVA with Tukey post-hoc. Significance was
944 defined as $p \leq 0.05$ (*), $p \leq 0.001$ (***), and not significant as $p > 0.05$ (ns).

945

946

947

948

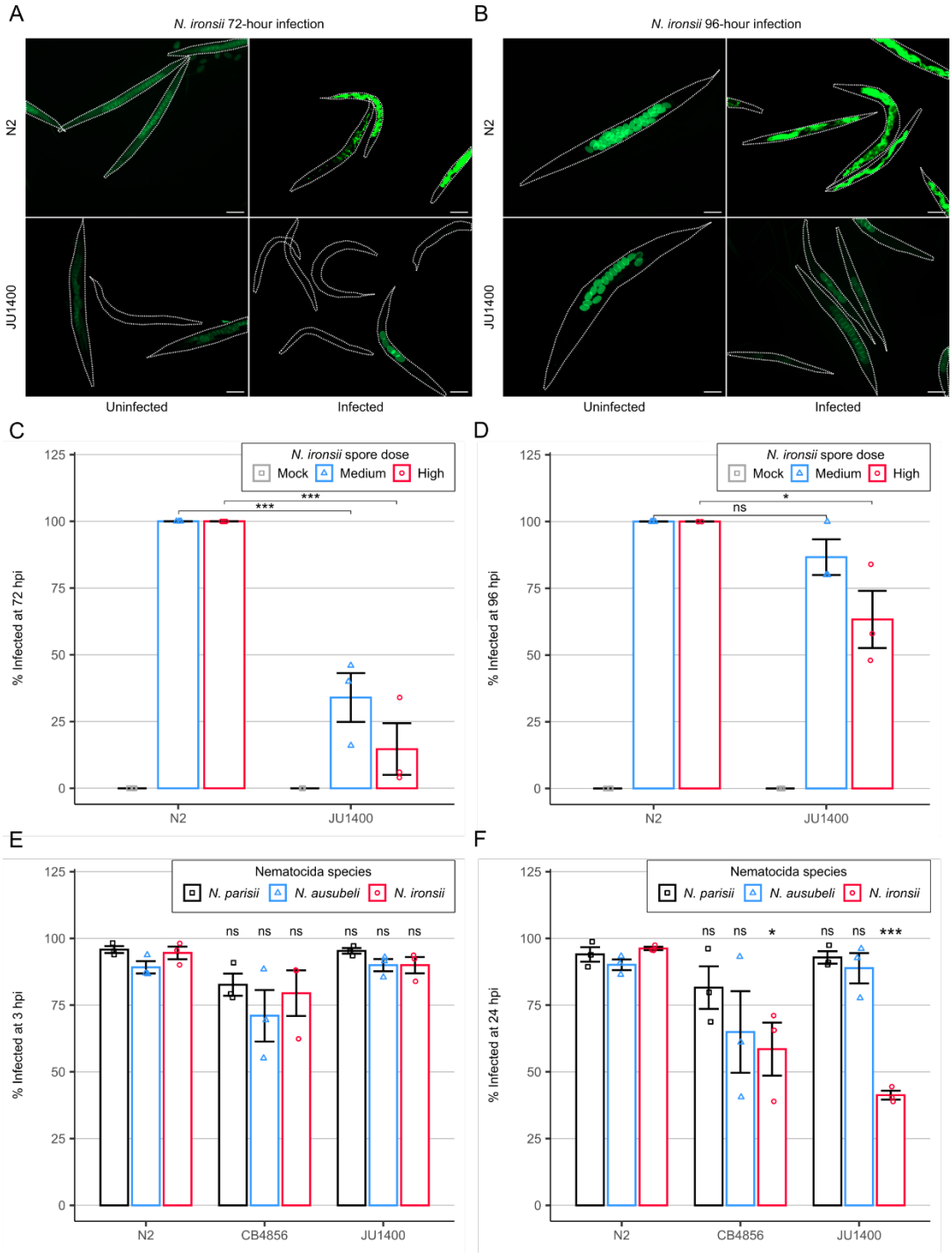

Figure S9. JU1400 is resistant to infection by *N. ironsii*. N2 and JU1400 L1 stage animals were infected with mock, medium, and high doses of *N. ironsii* for 72 (A and C) and 96 (B and D) hours and fixed. Embryos and mature spores are visualized by staining with DY96 (green), meronts are stained by a 18S rRNA FISH probe. (A-B) Representative images of high dose

954 infection from each experiment. Scale bars are 100 μm. (C-D) Barplots with SEM bars of percent
955 population with meronts visible. Data in (C, D) is combined from three biological replicates each
956 with n={47,50} worms per replicate. (E-F) N2, JU1400, and CB4856 animals at the L1 stage were
957 infected for 3 hours with 1.25 million spores of either *N. parisii*, *N. ausubeli*, or *N. ironsii* before
958 washing away excess spores. Animals were either fixed at 3 hours (E) or replated for an additional
959 21 hours (F) and then fixed. Shown are barplots with SEM bars of percent population with meronts
960 visible. Data in (E, F) are combined from three biological replicates each with n={59,179} worms
961 per replicate. p-values were determined by two-way ANOVA with Tukey post-hoc. Significance
962 was defined as $p \leq 0.05$ (*), $p \leq 0.001$ (***), and not significant as $p > 0.05$ (ns).

963

964

965

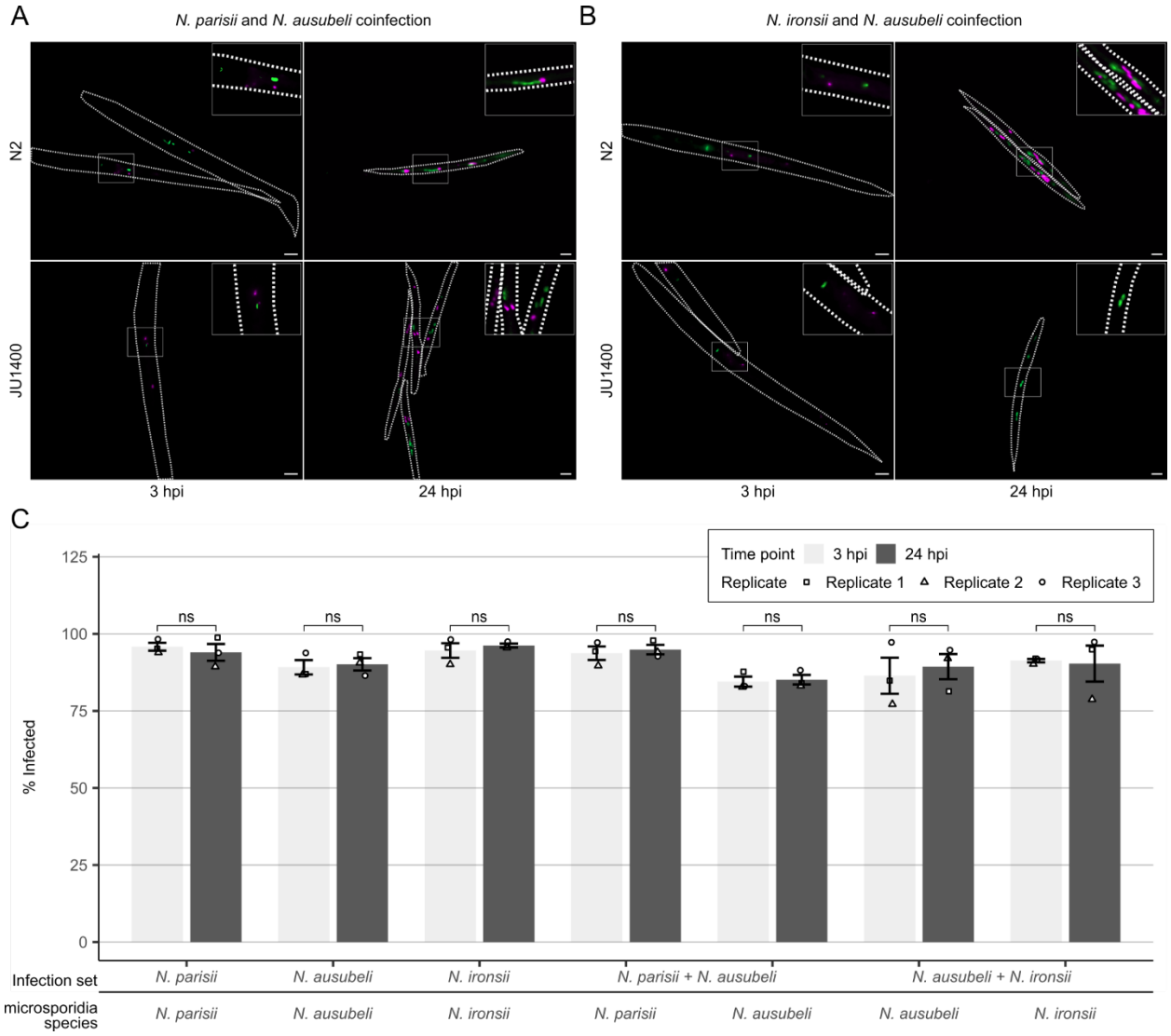

Figure S10. JU1400, but not N2, can specifically eliminate *N. ironsii* infection. N2 and JU1400 animals at the L1 stage were pulse infected for 3 hours with *N. parisii*, *N. ausubeli*, *N. ironsii, N. parisii* + *N. ausubeli, or N. ausubeli* + *N. ironsii* before washing away excess spores. Animals were either fixed immediately at 3 hpi or at 24 hpi. Samples were then stained with species-specific 18S RNA FISH probes (*N. ausubeli* = green; *N. parisii* and *N. ironsii* = magenta) and animals containing either sporoplasms or meronts were counted as infected. (A) Representative images of N2 and JU1400 infected with *N. parisii* and *N. ausubeli* (A) and *N. ironsii* and *N. ausubeli* (B). Scale bar 10 µm for 3 hpi and 25 µm for 24 hpi. Insets at top right for each

975 image show a zoomed in image of the outlined boxes. (C) Barplot with SEM bars show percent
976 of N2 animals infected per replicate from three biological replicates with n={59, 179} worms per
977 replicate. p-values were determined by two-way ANOVA with Tukey post-hoc. Non-significance
978 was defined as p > 0.05 (ns).

979

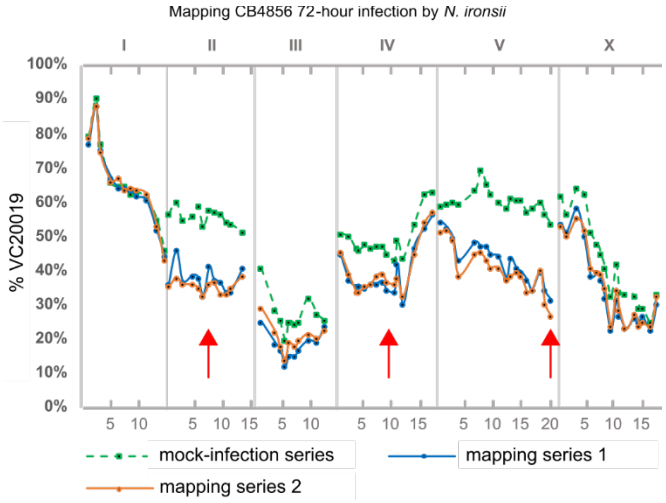

980

981 **Figure S11. Genetic mapping of CB4856 resistance to *N. ironsii*.** Genetic mapping of CB4856
982 resistance to N. ironsii was performed with MIP-MAP using the AWR133 mapping strain. Green
983 square-points and dotted lines represent a mock-infection replicate with the solid blue and orange
984 lines representing two biological replicates exposed to high dose infection conditions for 72-hours
985 per selection cycle. A red arrow on chromosome V indicates a strong signal on the right arm.
986 Additional red arrows on chromosomes II and IV indicate broad regions of interest across the
987 chromosomes that may contribute to CB4856 resistance phenotypes.

988

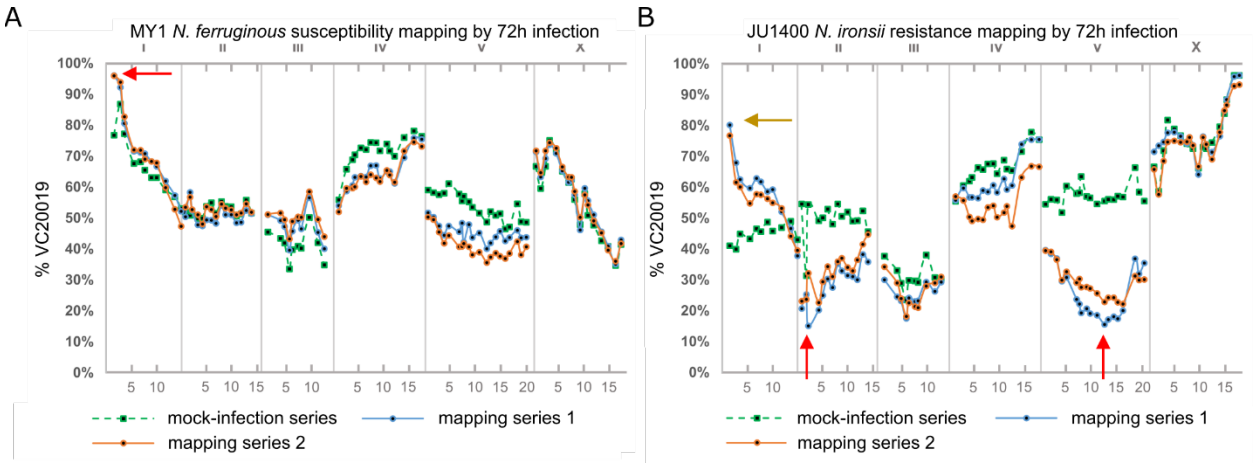

989

990 **Figure S12. Genetic mapping of interaction phenotypes of JU1400 to *N. ironsii* and MY1 to**
991 ***N. ferruginous* using 72-hour selections.** Genetic mapping of (A) JU1400 resistance to *N.*
992 *ironsii* and (B) MY1 susceptibility to *N. ferruginous* was performed with MIP-MAP using the
993 AWR133 mapping strain. Green square-points and dotted lines represent a mock-infection
994 replicate with the solid blue and orange lines representing two biological replicates exposed to
995 specific infection conditions. Red arrows indicate candidate regions of interest based on the
996 expected genome fixation direction during phenotype selection. Golden arrow indicates the *zeel-*
997 *1/peel-1* incompatibility locus at chromosome I.

998

999

1000

1001

1002

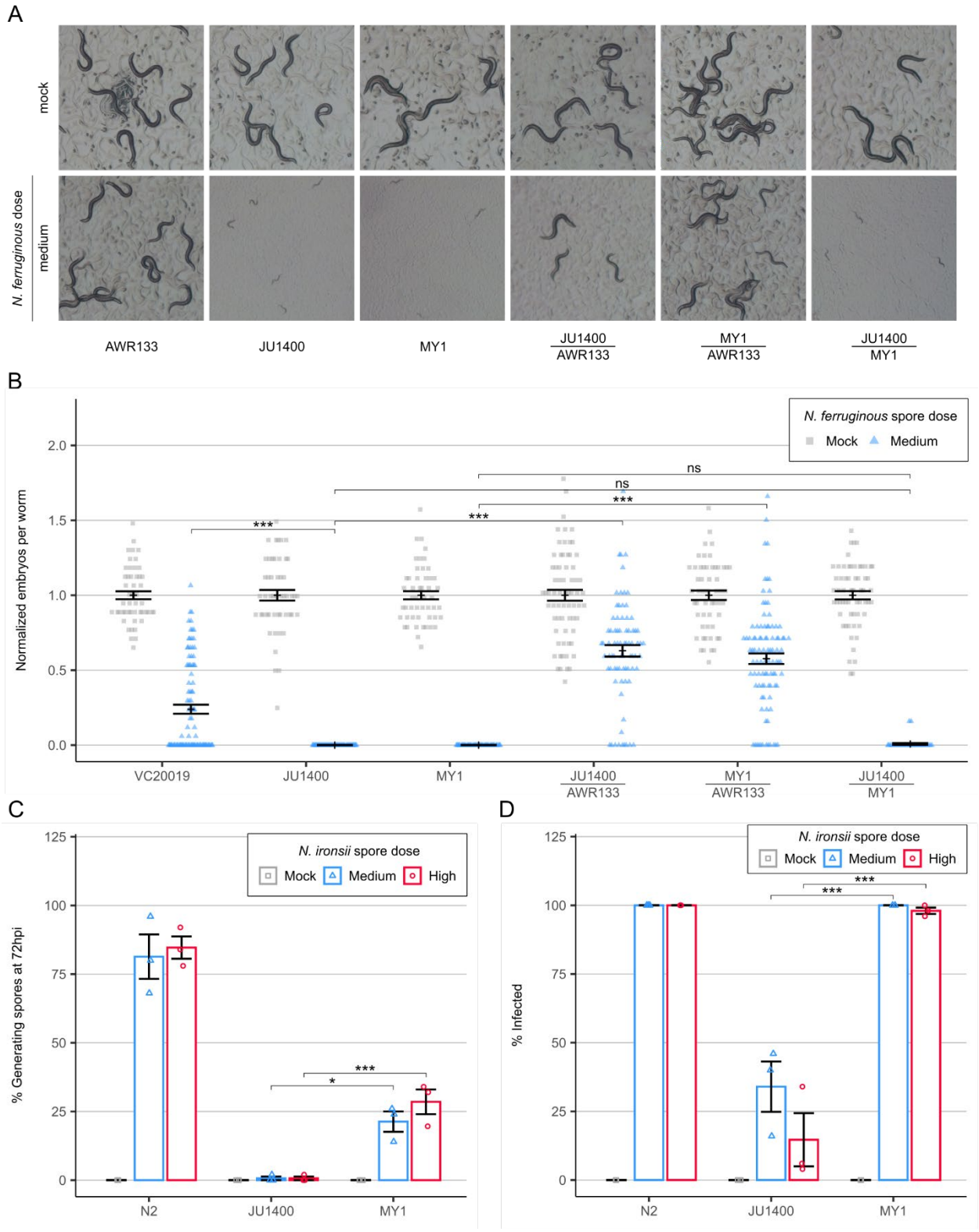

1003

1004 **Figure S13. JU1400 and MY1 susceptibility to *N. ferruginous* is recessive and MY1 is less**

1005 **resistant than JU1400 to *N. ironsii*.** (A-B) Analysis of F1 progeny from crosses between

1006 AWR133 (VC20019 with integrated pmyo-2::GFP) and the wild isolates JU1400 or MY1 as well
1007 as F1 progeny from crosses between JU1400 hermaphrodites and MY1 males. F1s were
1008 examined 72 hours post-infection by *N. ferruginous* for body size (A) and normalized embryo
1009 counts (B). B) Dotplot with mean and SEM bars of normalized embryo counts from infected
1010 populations with a minimum of n={47,51} worms per sample. (C-D). L1 stage animals were
1011 infected for 72 hours with *N. ironsii*, fixed, and stained with DY96 and an 18S rRNA FISH probe.
1012 Barplots depict the percent of animals with newly generated spores (C) or meront signal (D). p-
1013 values denote comparison to N2 controls and were determined by two-way ANOVA with Tukey
1014 post-hoc. Significance was defined as $p \leq 0.001$ (***), $p \leq 0.05$ (*) and not significant as $p > 0.05$
1015 (ns).

1016

1017

1018

1019

1020

1021

1022

1023

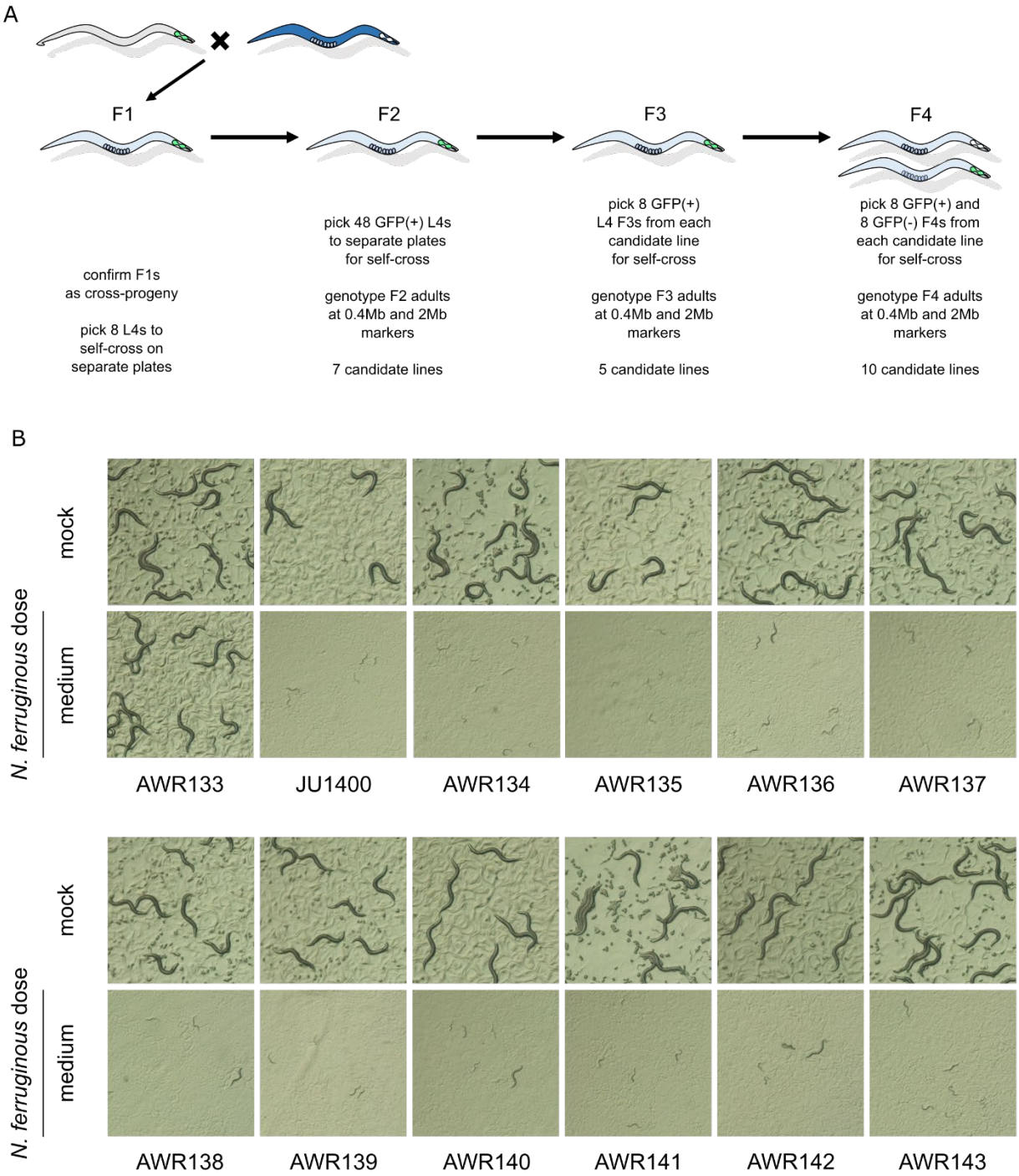

Figure S14. Generation of near-isogenic lines carrying the chromosome I region that is responsible for susceptibility to *N. ferruginous*. A schematic (A) of 10 separate near-isogenic lines generated through a cross between AWR133 and JU1400. These lines were infected with a

1028 medium dose of *N. ferruginous* for 72 hours (B) and their resulting body size phenotype was
1029 assessed in comparison to N2 and JU1400 control strains.

1030

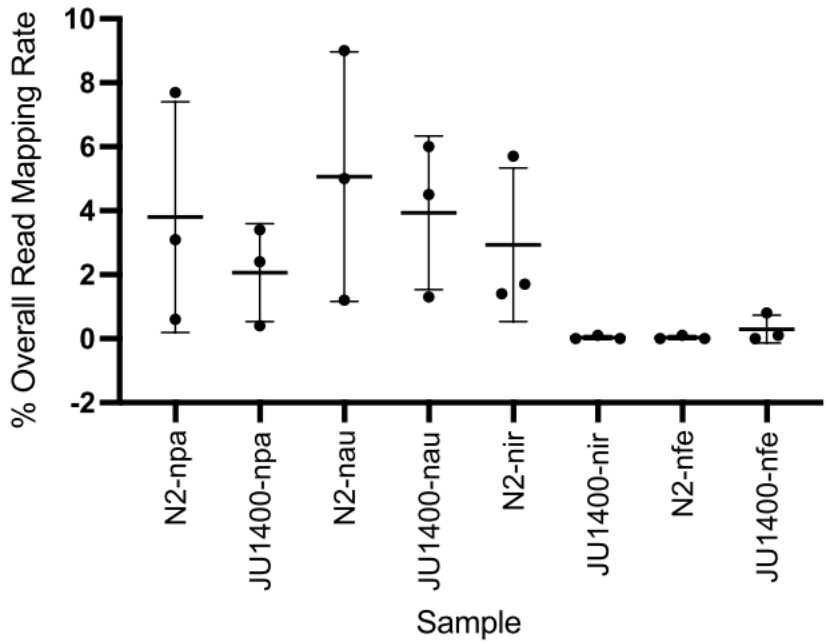

1031

1032 **Figure S15. Microsporidia mRNA reads per sample demonstrates JU1400 resistance to *N.***
1033 ***ironsii*.** Scatterplot of overall read mapping rate of *Nematocida* in both strains with mean and
1034 standard deviation. uni (uninfected), npa (*N. parisii)*, nau (*N. ausubeli*), nir (*N. ironsii),* and nfe (*N.*
1035 *ferruginous)*.

A

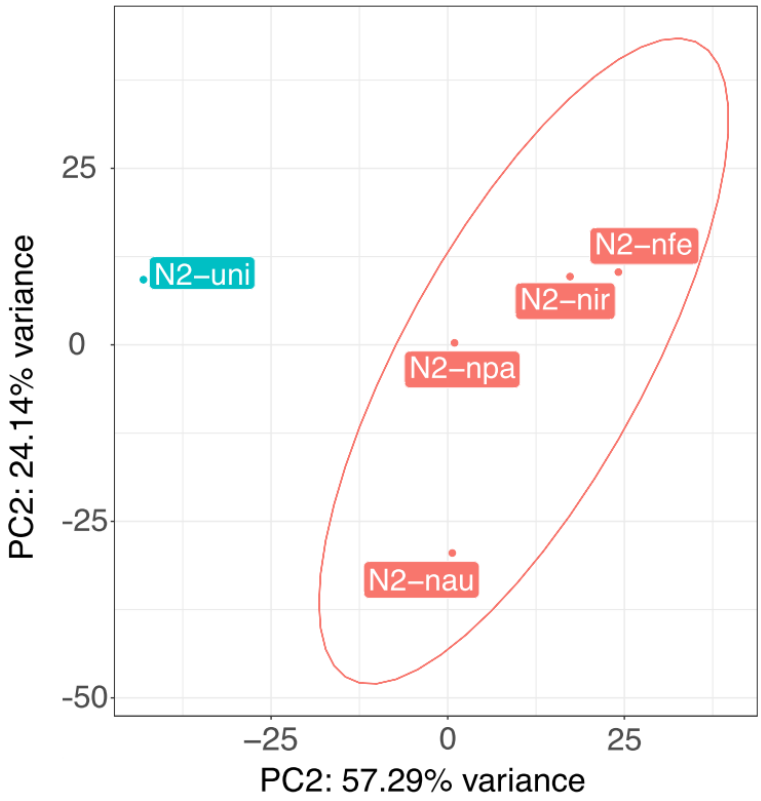

B

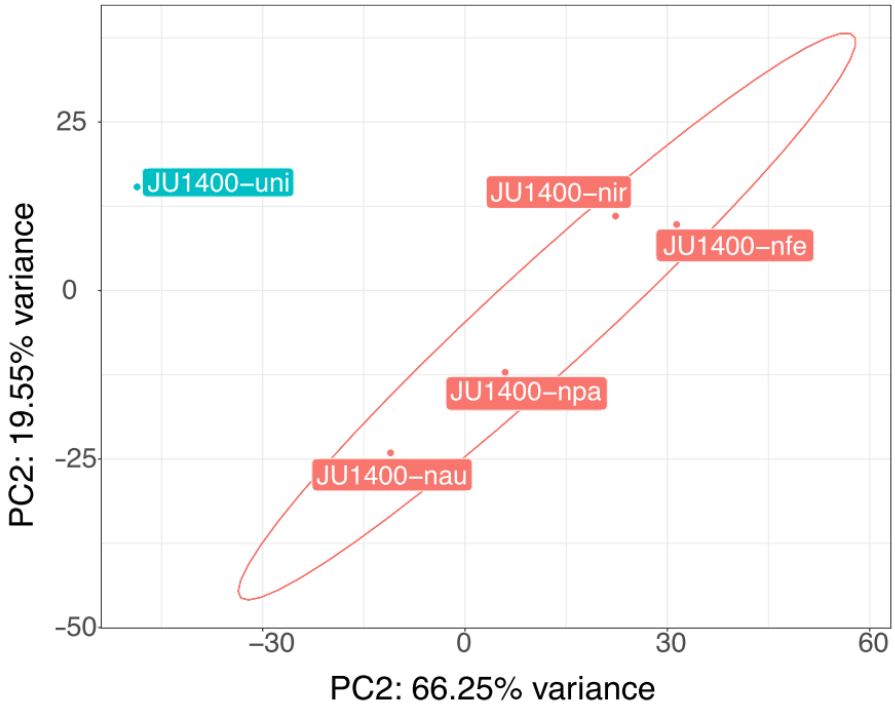

Infection: Infected Uninfected

1036

1037 **Figure S16. Principal component analysis of N2 and JU1400 samples.** Principal component
1038 plots of expression data from only (A) N2 samples or (B) JU1400 samples. Circles represent
1039 confidence ellipses around each strain at 95% confidence interval. uni (uninfected), npa (*N.*
1040 *parisii)*, nau (*N. ausubeli*), nir (*N. ironsii),* and nfe (*N. ferruginous)*.

1041

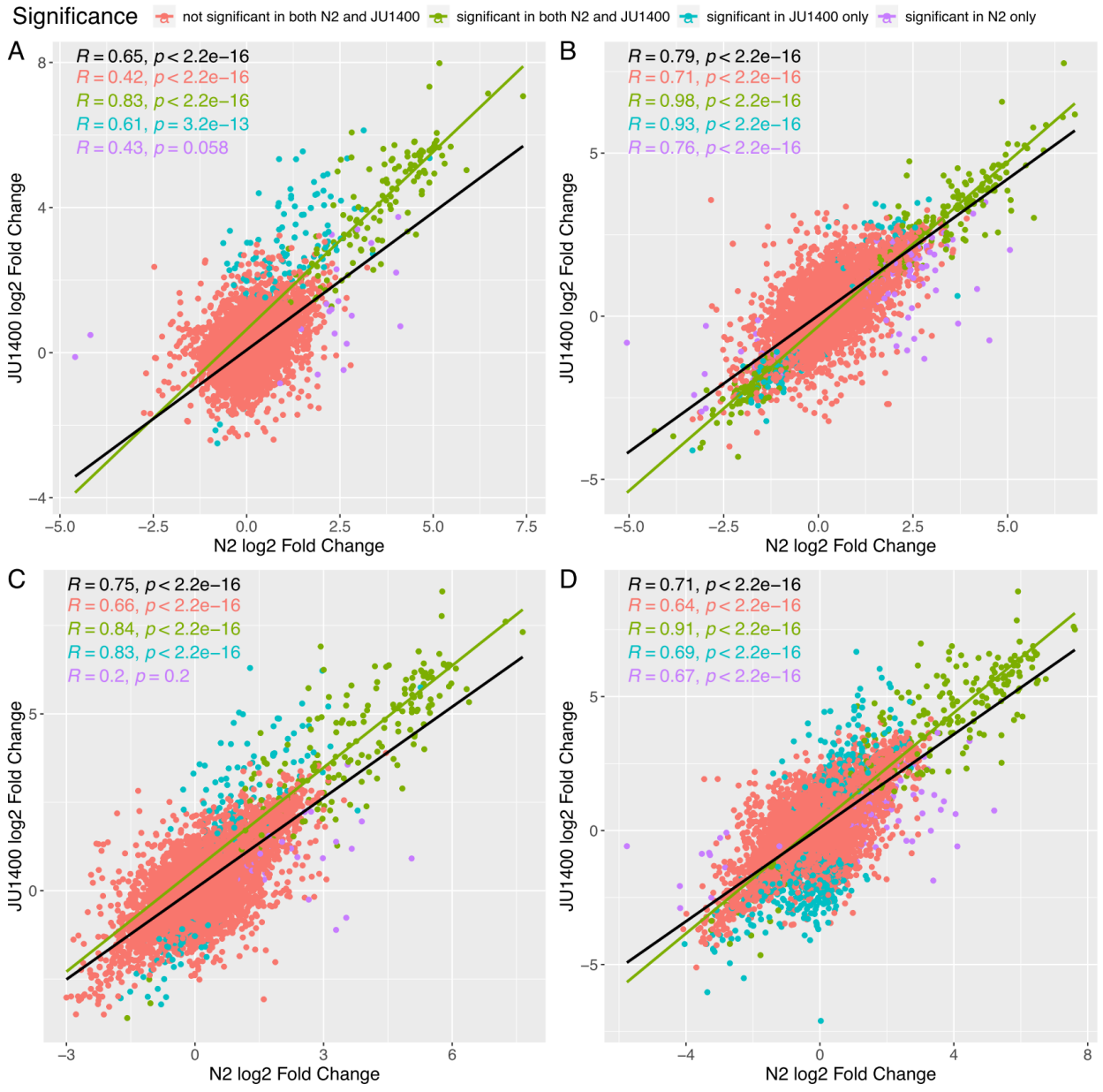

1042

1043 **Figure S17. Comparison of correlation between N2 and JU1499 strains after infection with**
1044 **different microsporidia species.** Correlation between log2 fold changes in genes of N2 and
1045 JU1400 animals infected with (A) *N. parisii* (B) *N. ausubeli* (C) *N. ironsii* (D) *N. ferruginous*.
1046 Pearson's correlation value and p-value for each cluster (pink, green, blue, purple) are presented
1047 in the upper left corner. Pearson's correlation value and p-value for all the genes are presented
1048 in the bottom left corner. A gene with FDR adjusted p-value of <0.01 is deemed significant in each
1049 strain.

1050

1051

1052

1053

1054

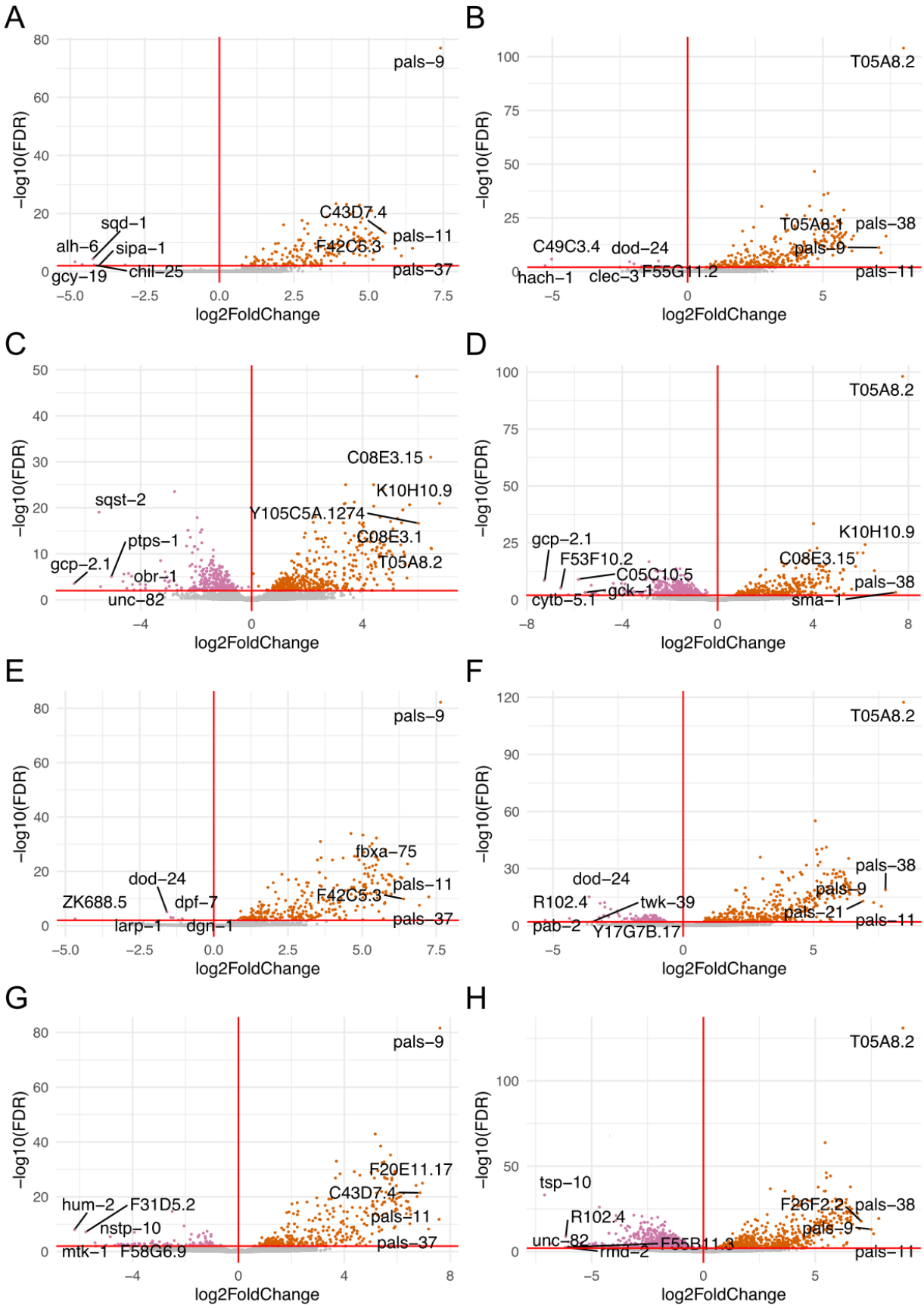
A
pals−9
sqd−1
alh−6
sipa−1
gcy−19
chil−25
C43D7.4
F42C5.3
pals−11
pals−37
−log10(FDR)
log2FoldChange
B
T05A8.2
T05A8.1
pals−38
pals−9
C49C3.4
dod−24
hach−1
clec−3
F55G11.2
pals−11
C
C08E3.15
K10H10.9
sqst−2
Y105C5A.1274
C08E3.1
ptps−1
T05A8.2
gcp−2.1
obr−1
unc−82
D
T05A8.2
K10H10.9
gcp−2.1
F53F10.2
C05C10.5
C08E3.15
pals−38
gck−1
cytb−5.1
sma−1
E
pals−9
fbxa−75
dod−24
pals−11
ZK688.5
dpf−7
F42C5.3
larp−1
dgn−1
pals−37
F
T05A8.2
pals−38
dod−24
pals−9
R102.4
twk−39
pals−21
pab−2
Y17G7B.17
pals−11
G
pals−9
F20E11.17
C43D7.4
hum−2
F31D5.2
pals−11
nstp−10
pals−37
mtk−1
F58G6.9
H
T05A8.2
tsp−10
F26F2.2
pals−38
R102.4
pals−9
unc−82
rmd−2
F55B11.3
pals−11

1055

1056

1057 **Figure S18. Volcano plots of differentially regulated genes.** (A) *N. parisii*-infected N2. (B) *N.*
1058 *parisii*-infected JU1400. (C) *N. ausubeli*-infected N2. (D) *N. ausubeli*-infected JU1400. (E) *N.*
1059 *ironsii*-infected N2. (F) *N. ironsii*-infected JU1400. (G) *N. ferruginous*-infected N2. (H) *N.*
1060 *ferruginous*-infected JU1400. Each point represents a gene, orange points indicate differentially
1061 upregulated genes, pink points are differentially downregulated genes while grey points represent
1062 genes with FDR-adjusted p-value >0.01 (red horizontal line). The top five differentially
1063 upregulated and downregulated genes with FDR-adjusted p-value <0.01 are labelled with their
1064 respective gene names.

1065

1066

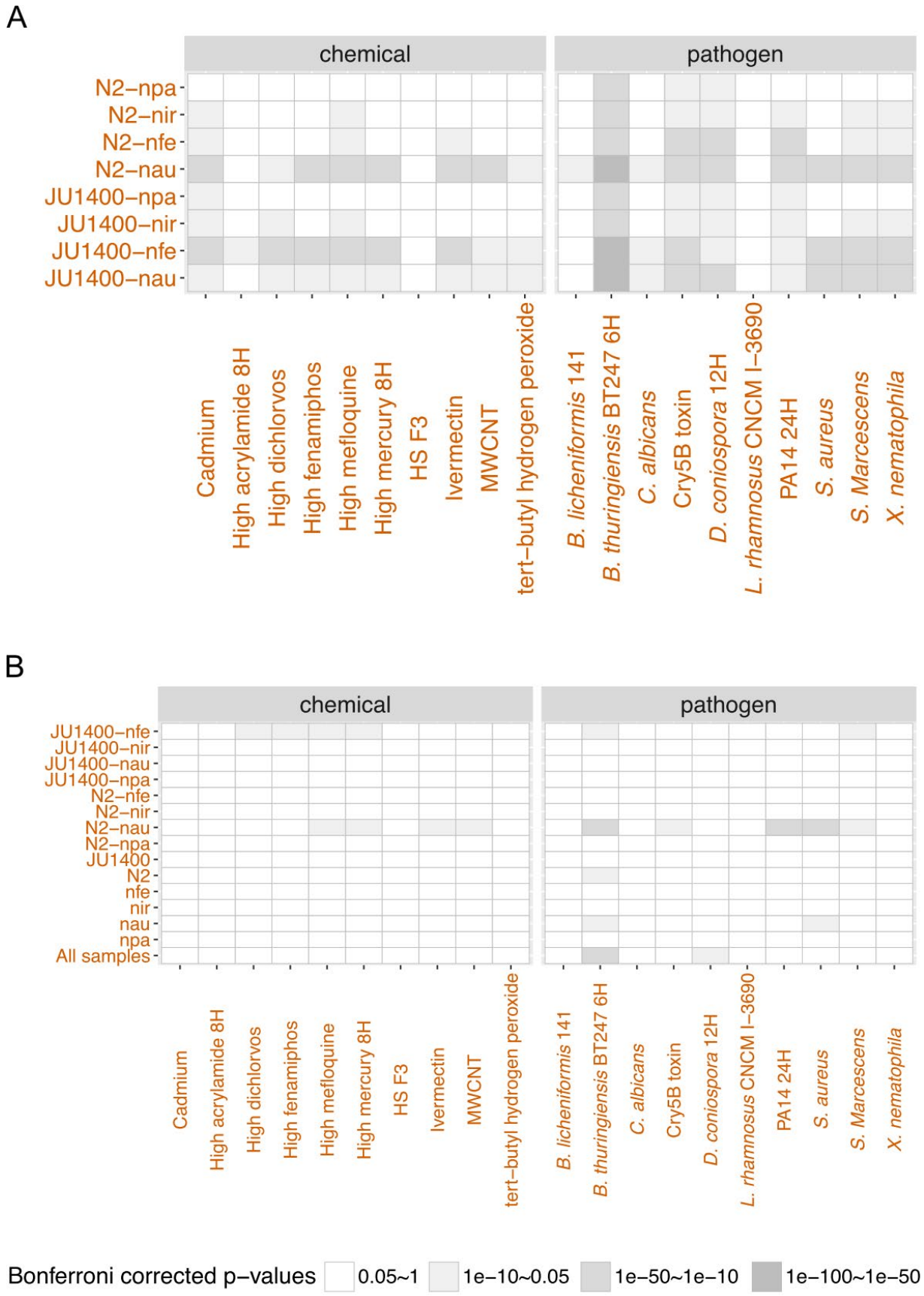
A
chemical
pathogen
N2−npa
N2−nir
N2−nfe
N2−nau
JU1400−npa
JU1400−nir
JU1400−nfe
JU1400−nau
Cadmium
High acrylamide 8H
High dichlorvos
High fenamiphos
High mefloquine
High mercury 8H
HS F3
Ivermectin
MWCNT
tert−butyl hydrogen peroxide
B. licheniformis 141
B. thuringiensis BT247 6H
C. albicans
Cry5B toxin
D. coniospora 12H
L. rhamnosus CNCM I−3690
PA14 24H
S. aureus
S. Marcescens
X. nematophila
B
chemical
pathogen
JU1400−nfe
JU1400−nir
JU1400−nau
JU1400−npa
N2−nfe
N2−nir
N2−nau
N2−npa
JU1400
N2
nfe
nir
nau
npa
All samples
Cadmium
High acrylamide 8H
High dichlorvos
High fenamiphos
High mefloquine
High mercury 8H
HS F3
Ivermectin
MWCNT
tert−butyl hydrogen peroxide
B. licheniformis 141
B. thuringiensis BT247 6H
C. albicans
Cry5B toxin
D. coniospora 12H
L. rhamnosus CNCM I−3690
PA14 24H
S. aureus
S. Marcescens
X. nematophila
Bonferroni corrected p−values
0.05~1
1e−10~0.05
1e−50~1e−10
1e−100~1e−50

1067

1068 **Figure S19. Overlap between the significant upregulated genes upon microsporidia**
1069 **infection and differentially expressed datasets of *C. elegans* genes upon exposure to**
1070 **chemicals or bacterial infection.** (A) upregulated genes from microsporidia-infected samples.
1071 (B) upregulated gens from strain specific, pathogen specific, and strain-pathogen specific gene
1072 sets. 'npa' indicates infection by *N. parisii*, 'nau' indicates infection by *N. ausubeli*, 'nir' indicates
1073 infection by *N. ironsii* while 'nfe indicates infection by *N. ferruginous*.

1074

1075

1076

1077

1078

1079

1080

1081

1082

1083

1084

1085

1086

1087

1088

1089 **Table 1. PhenoMIP screen interaction hits**

Strain	Site of isolation	Microsporidia species	Interaction	Modified z-score	Single infection embryo phenotype?
AB1	Adelaide, Australia	*N. ferruginous*	Resistance	1.65, 1.64	Yes
JU397	Ouistreham, France	*N. ferruginous*	Resistance	2.58, 2.59	Yes
LKC34	Antananarivo, Madagascar	*N. ferruginous*	Resistance	2.14, 2.40	N/A
ED3040	Johannesburg, South Africa	*N. ferruginous*	Susceptibility	-1.90, -1.90	N/A
ED3042	Capetown, South Africa	*N. ferruginous*	Susceptibility	-2.53, -1.57	Yes
JU360	Franconville, France	*N. ferruginous*	Susceptibility	-2.68, -2.74	Yes
MY1	Munster, Germany	*N. ferruginous*	Susceptibility	-6.05, -6.05 -4.52, -4.25 -2.17. -1.85	Yes
JU1400	Sevilla, Spain	*N. ferruginous*	Susceptibility	-6.43, -6.43 -3.33, -3.33	Yes
CB4856	Hawaii, USA	*N. ironsii*	Resistance	2.48, 2.88	Yes
JU300	Le Blanc, France	*N. ironsii*	Resistance	2.19, 2.70	No
MY2	Munster, Germany	*N. ironsii*	Susceptibility	-2.83, -3.50	Yes
JU533	Primel-Tregastel, France	*N. ironsii*	Susceptibility	-2.00, -2.00	N/A
JU642	Paris, France	*N. ironsii*	Susceptibility	-2.44, -3.06	N/A
JU1400	Sevilla, Spain	*N. ironsii*	Susceptibility	-1.78, -1.78	Yes
JU360	Franconville, France	*N. ausubeli*	Resistance	2.03, 1.88	No
MY2	Munster, Germany	*N. ausubeli*	Susceptibility	-2.07, -2.42	No

1090

1091

1092

1093 **Table S1. Microsporidia species information**

Microsporidia species	Original host	Infected tissue	Geographical origin
Nematocida parisii[53]	*C. elegans*	Intestine	France
Nematocida ausubeli[53,65]	*C. briggsae*	Intestine	India
Nematocida ironsii[42,51]	*C. briggsae*	Intestine	Hawaii
Nematocida ferruginous[43]	*C. elegans* (likely)	Epidermis/muscle	France

1094

1095 **Table S2. PhenoMIP microsporidia infection doses**

Microsporidia species	Microsporidia strain	Infection round	Spores per cm^2 media Low	Medium	High
Nematocida parisii	ERTm1	1	8,000	16,000	32,000
		2-4	13,269	26,539	53,078
		Follow-up infections		***26,539***	***53,078***
Nematocida ausubeli	ERTm2	1	26,539	NA	53,078
		2-4	26,539	39,808	53,078
		Follow-up infections		***17,692***	***53,078***
Nematocida ironsii	ERTm5	1	22,116	44,232	88,464
		2-4	30,692	61,924	123,849
		Follow-up infections		***61,924***	***123,849***
Nematocida ferruginous	LUAm1	1	88,464	176,928	353,857
		2-3	159,235	318,471	636,942
		4	159,235	318,471	751,592
		Follow-up infections		***318,471***	***751,592***
	LUAm3	***Follow-up infections***		***353,857***	
Nematocida cider	AWRm77	***Follow-up infections***		***141,542***	

1096 * effective dose of spores used in retests and additional infections

1097

1098 **Table S3. Wild isolate mapping microsporidia infection doses**

Wild isolate strain(s)	Microsporidia strain	Infection time (hours)	Infection round	Spores per cm^2 media
JU1400, MY1	*Nematocida ferruginous*	72	1-2	350,318
			3	445,859
JU1400	*Nematocida ironsii*	72	1	178,343
			2-3	254,777
JU1400	*Nematocida ironsii*	96	1-2	509,554

CB4856	*Nematocida ironsii*	72	1	178,343
			2-3	254,777

1099

1100 **Table S4. NIL strain chromosome I region composition**

Strain	I:491,763	I:1,051,810	I:1,567,450	I:2,012,869	GFP Status I-2,851,135
AWR134	JU1400	JU1400	JU1400	--	+
AWR135	JU1400	JU1400	JU1400	JU1400	-
AWR136	JU1400	JU1400	JU1400	JU1400	+
AWR137	JU1400	JU1400	JU1400	JU1400	-
AWR138	JU1400	--	--	--	+
AWR139	JU1400	JU1400	JU1400	JU1400	-
AWR140	JU1400	JU1400	--	--	+
AWR141	JU1400	JU1400	JU1400	JU1400	-
AWR142	JU1400	JU1400	--	--	+
AWR143	JU1400	JU1400	JU1400	JU1400	-

1101

1102 **Table S10. Gene classes and domains used for enrichment analyses.**

1103

Domain/ Gene Family	Databse	Wormbase gene class OR Pfam ID
F-box	Wormbase	fbxa, fbxb, fbxc
MATH (meprin or Traf homology) or BATH (BTB and MATH domain-containing)	Wormbase	math, bath
PALS (protein containing ALS2CR12 signature)	Wormbase	pals
C-type lectins	Wormbase	clec
DUF713	Pfam	PF015218
DUF684	Pfam	PF05075
chil	Wormbase	chil
Histone	Pfam	PF00125
Nematode cuticle collagen N-terminal domain	Pfam	PF01484
skr (Skp1-related)	Wormbase	Skr
Other (Any genes not in the domain or gene family above)	-	-

1104

1105

1106

1107

1108

1109 **References**

1110 1. Band G, Rockett KA, Spencer CCA, Kwiatkowski DP. A novel locus of resistance to severe malaria in
1111 a region of ancient balancing selection. Nature. 2015;526: 253–257. doi:10.1038/nature15390

1112 2. Samson M, Libert F, Doranz BJ, Rucker J, Liesnard C, Farber CM, et al. Resistance to HIV-1 infection
1113 in caucasian individuals bearing mutant alleles of the CCR-5 chemokine receptor gene. Nature.
1114 1996;382: 722–725. doi:10.1038/382722a0

1115 3. Sabeti PC, Schaffner SF, Fry B, Lohmueller J, Varilly P, Shamovsky O, et al. Positive natural selection
1116 in the human lineage. Science. 2006;312: 1614–1620. doi:10.1126/science.1124309

1117 4. Lazzaro BP, Sceurman BK, Clark AG. Genetic Basis of Natural Variation in D. melanogaster
1118 Antibacterial Immunity. Science. 2004;303: 1873–1876. doi:10.1126/science.1092447

1119 5. Duxbury EM, Day JP, Maria Vespasiani D, Thüringer Y, Tolosana I, Smith SC, et al. Host-pathogen
1120 coevolution increases genetic variation in susceptibility to infection. eLife. 2019;8: 1–21.
1121 doi:10.7554/eLife.46440

1122 6. Lazzaro BP, Sackton TB, Clark AG. Genetic variation in Drosophila melanogaster resistance to
1123 infection: A comparison across bacteria. Genetics. 2006;174: 1539–1554.
1124 doi:10.1534/genetics.105.054593

1125 7. Schulenburg H, Ewbank JJ. Diversity and specificity in the interaction between Caenorhabditis
1126 elegans and the pathogen Serratia marcescens. BMC Evolutionary Biology. 2004;4: 49.
1127 doi:10.1186/1471-2148-4-49

1128 8. Marquet S. Overview of human genetic susceptibility to malaria: From parasitemia control to
1129 severe disease. Infect Genet Evol. 2018;66: 399–409. doi:10.1016/j.meegid.2017.06.001

1130 9. Raberg L, Sim D, Read AF. Disentangling genetic variation for resistance and tolerance to infectious
1131 diseases in animals. Science. 2007;318: 812–814. doi:10.1126/science.1148526

1132 10. Medzhitov R, Schneider DS, Soares MP. Disease tolerance as a defense strategy. Science.
1133 2012;335: 936–941. doi:10.1126/science.1214935

1134 11. Wadi L, Reinke AW. Evolution of microsporidia: An extremely successful group of eukaryotic
1135 intracellular parasites. PLoS Pathog. 2020;16: e1008276. doi:10.1371/journal.ppat.1008276

1136 12. Stentiford GD, Feist SW, Stone DM, Bateman KS, Dunn AM. Microsporidia: diverse, dynamic, and
1137 emergent pathogens in aquatic systems. Trends Parasitol. 2013;29: 567–578.
1138 doi:10.1016/j.pt.2013.08.005

1139 13. Murareanu BM, Sukhdeo R, Qu R, Jiang J, Reinke AW, Weiss LM. Generation of a Microsporidia
1140 Species Attribute Database and Analysis of the Extensive Ecological and Phenotypic Diversity of
1141 Microsporidia. mBio. 2021. pp. e01490-21.

1142 14. Willis AR, Reinke AW. Factors That Determine Microsporidia Infection and Host Specificity. Exp
1143 Suppl. 2022;114: 91–114. doi:10.1007/978-3-030-93306-7_4

1144 15. Troemel ER, Felix M-A, Whiteman NK, Barriere A, Ausubel FM. Microsporidia are natural
1145 intracellular parasites of the nematode Caenorhabditis elegans. PLoS Biol. 2008;6: 2736–2752.
1146 doi:10.1371/journal.pbio.0060309

1147 16. Balla KM, Luallen RJ, Bakowski MA, Troemel ER. Cell-to-cell spread of microsporidia causes
1148 Caenorhabditis elegans organs to form syncytia. Nature Microbiology. 2016;1: 16144.

1149 17. Higes M, Martín-Hernández R, Botías C, Bailón EG, González-Porto AV, Barrios L, et al. How natural
1150 infection by Nosema ceranae causes honeybee colony collapse. Environ Microbiol. 2008;10: 2659–
1151 2669. doi:10.1111/j.1462-2920.2008.01687.x

1152 18. Richaud A, Zhang G, Lee D, Lee J, Félix M-A. The Local Coexistence Pattern of Selfing Genotypes in
1153 Caenorhabditis elegans Natural Metapopulations. Genetics. 2018;208: 807–821.
1154 doi:10.1534/genetics.117.300564

1155 19. Balla KM, Andersen EC, Kruglyak L, Troemel ER. A Wild C. Elegans Strain Has Enhanced Epithelial
1156 Immunity to a Natural Microsporidian Parasite. PLoS Pathogens. 2015;11: e1004583.
1157 doi:10.1371/journal.ppat.1004583

1158 20. Tamim El Jarkass H, Mok C, Schertzberg MR, Fraser AG, Troemel ER, Reinke AW. An intestinally
1159 secreted host factor promotes microsporidia invasion of C. elegans. Lourido S, Sengupta P, editors.
1160 eLife. 2022;11: e72458. doi:10.7554/eLife.72458

1161 21. Capaul M, Ebert D. Parasite-Mediated Selection in Experimental Daphnia Magna Populations.
1162 Evolution. 2003;57: 249–260. doi:10.1111/j.0014-3820.2003.tb00260.x

1163 22. Haag CR, Ebert D. Parasite–mediated selection in experimental metapopulations of Daphnia
1164 magna. Proceedings of the Royal Society of London Series B: Biological Sciences. 2004;271: 2149–
1165 2155. doi:10.1098/rspb.2004.2841

1166 23. Huang Q, Lattorff HMG, Kryger P, Conte YL, Moritz RFA. A selective sweep in a microsporidian
1167 parasite Nosema-tolerant honeybee population, Apis mellifera. Animal Genetics. 2014;45: 267–
1168 273. doi:10.1111/age.12114

1169 24. Keller D, Kirk D, Luijckx P. Four QTL underlie resistance to a microsporidian parasite that may drive
1170 genome evolution in its Daphnia host. bioRxiv. 2019; 847194. doi:10.1101/847194

1171 25. Krebs M, Routtu J, Ebert D. QTL mapping of a natural genetic polymorphism for long-term parasite
1172 persistence in Daphnia populations. Parasitology. 2017;144: 1686–1694.
1173 doi:10.1017/S0031182017001032

1174 26. Routtu J, Ebert D. Genetic architecture of resistance in Daphnia hosts against two species of host-
1175 specific parasites. Heredity (Edinb). 2015;114: 241–248. doi:10.1038/hdy.2014.97

1176 27. King KC, Brockhurst MA, Vasieva O, Paterson S, Betts A, Ford SA, et al. Rapid evolution of microbe-
1177 mediated protection against pathogens in a worm host. The ISME Journal. 2016;10: 1915–1924.
1178 doi:10.1038/ismej.2015.259

1179 28. Morran LT, Schmidt OG, Gelarden IA, Parrish RC, Lively CM. Running with the Red Queen: Host-
1180 Parasite Coevolution Selects for Biparental Sex. Science. 2011;333: 216–218.
1181 doi:10.1126/science.1206360

1182 29. Papkou A, Guzella T, Yang W, Koepper S, Pees B, Schalkowski R, et al. The genomic basis of Red
1183 Queen dynamics during rapid reciprocal host–pathogen coevolution. PNAS. 2019;116: 923–928.
1184 doi:10.1073/pnas.1810402116

1185 30. Masri L, Branca A, Sheppard AE, Papkou A, Laehnemann D, Guenther PS, et al. Host–Pathogen
1186 Coevolution: The Selective Advantage of Bacillus thuringiensis Virulence and Its Cry Toxin Genes.
1187 PLOS Biology. 2015;13: e1002169. doi:10.1371/journal.pbio.1002169

1188 31. Schulenburg H, Félix M-A. The Natural Biotic Environment of . Genetics. 2017;206: 55–86.

1189 32. Zhang G, Sachse M, Prevost M-C, Luallen RJ, Troemel ER, Felix M-A. A Large Collection of Novel
1190 Nematode-Infecting Microsporidia and Their Diverse Interactions with Caenorhabditis elegans and
1191 Other Related Nematodes. PLoS Pathog. 2016;12: e1006093. doi:10.1371/journal.ppat.1006093

1192 33. Cook DE, Zdraljevic S, Roberts JP, Andersen EC. CeNDR, the Caenorhabditis elegans natural
1193 diversity resource. Nucleic Acids Research. 2017. doi:10.1093/nar/gkw893

1194 34. Ashe A, Bélicard T, Le Pen J, Sarkies P, Frézal L, Lehrbach NJ, et al. A deletion polymorphism in the
1195 Caenorhabditis elegans RIG-I homolog disables viral RNA dicing and antiviral immunity. eLife.
1196 2013;2013: 1–21. doi:10.7554/eLife.00994.001

1197 35. Sterken MG, Sluijs L van, Wang YA, Ritmahan W, Gultom ML, Riksen JAG, et al. Punctuated loci on
1198 chromosome IV determine natural variation in Orsay virus susceptibility of Caenorhabditis elegans
1199 strains Bristol N2 and Hawaiian CB4856. bioRxiv. 2020; 2020.10.30.361683.
1200 doi:10.1101/2020.10.30.361683

1201 36. Reddy KC, Andersen EC, Kruglyak L, Kim DH. A Polymorphism in npr-1 Is a Behavioral Determinant
1202 of Pathogen Susceptibility in C. elegans. Science. 2009;323: 382–384. doi:10.1126/science.1166527

1203 37. Huang Y, Kammenga JE. Genetic Variation in Caenorhabditis elegans Responses to Pathogenic
1204 Microbiota. Microorganisms. 2020;8: 618. doi:10.3390/microorganisms8040618

1205 38. Webster AK, Hung A, Moore BT, Guzman R, Jordan JM, Kaplan REW, et al. Population Selection and
1206 Sequencing of Caenorhabditis elegans Wild Isolates Identifies a Region on Chromosome III
1207 Affecting Starvation Resistance. G3: Genes, Genomes, Genetics. 2019;9: 3477–3488.
1208 doi:10.1534/g3.119.400617

1209 39. Mok C, Belmarez G, Edgley ML, Moerman DG, Waterston RH. PhenoMIP: High-Throughput
1210 Phenotyping of Diverse Caenorhabditis elegans Populations via Molecular Inversion Probes. G3:
1211 Genes, Genomes, Genetics. 2020;10: 3977–3990. doi:10.1534/g3.120.401656

1212 40. Webster AK, Chitrakar R, Powell M, Chen J, Fisher K, Tanny R, et al. Natural variation in the
1213 irld gene family affects insulin/IGF signaling and starvation resistance. bioRxiv. 2021;
1214 2021.06.07.447366. doi:10.1101/2021.06.07.447366

1215 41. Luallen RJ, Reinke AW, Tong L, Botts MR, Felix M-A, Troemel ER. Discovery of a Natural
1216 Microsporidian Pathogen with a Broad Tissue Tropism in Caenorhabditis elegans. PLoS Pathog.
1217 2016;12: e1005724. doi:10.1371/journal.ppat.1005724

1218 42. Reinke AW, Balla KM, Bennett EJ, Troemel ER. Identification of microsporidia host-exposed
1219 proteins reveals a repertoire of rapidly evolving proteins. Nat Commun. 2017;8: 14023.
1220 doi:10.1038/ncomms14023

1221 43. Wadi L, Jarkass HTE, Tran, Tuan, Islah, Nizar, Luallen, Robert, Reinke AW. Genomic and phenotypic
1222 evolution of nematode-infecting microsporidia. In preparation. 2022.

1223 44. Jarkass HTE, Reinke AW. The ins and outs of host-microsporidia interactions during invasion,
1224 proliferation and exit. Cellular Microbiology. 2020;22: e13247. doi:10.1111/cmi.13247

1225 45. Tecle E, Troemel ER. Insights from C. elegans into Microsporidia Biology and Host-Pathogen
1226 Relationships. Exp Suppl. 2022;114: 115–136. doi:10.1007/978-3-030-93306-7_5

1227 46. Reddy KC, Dror T, Sowa JN, Panek J, Chen K, Lim ES, et al. An Intracellular Pathogen Response
1228 Pathway Promotes Proteostasis in C. elegans. Curr Biol. 2017;27: 3544-3553.e5.
1229 doi:10.1016/j.cub.2017.10.009

1230 47. Reddy KC, Dror T, Underwood RS, Osman GA, Elder CR, Desjardins CA, et al. Antagonistic paralogs
1231 control a switch between growth and pathogen resistance in C. elegans. PLoS Pathog. 2019;15:
1232 e1007528. doi:10.1371/journal.ppat.1007528

1233 48. Willis AR, Zhao W, Sukhdeo R, Wadi L, Jarkass HTE, Claycomb JM, et al. A parental transcriptional
1234 response to microsporidia infection induces inherited immunity in offspring. Science Advances.
1235 2021;7: eabf3114. doi:10.1126/sciadv.abf3114

1236 49. Tecle E, Chhan CB, Franklin L, Underwood RS, Hanna-Rose W, Troemel ER. The purine nucleoside
1237 phosphorylase pnp-1 regulates epithelial cell resistance to infection in C. elegans. PLOS Pathogens.
1238 2021;17: e1009350. doi:10.1371/journal.ppat.1009350

1239 50. Balla KM, Luallen RJ, Bakowski MA, Troemel ER. Cell-to-cell spread of microsporidia causes
1240 Caenorhabditis elegans organs to form syncytia. Nature Microbiology. 2016;1: 16144.

1241 51. Balla KM, Andersen EC, Kruglyak L, Troemel ER. A wild C. elegans strain has enhanced epithelial
1242 immunity to a natural microsporidian parasite. PLoS Pathog. 2015;11: e1004583.
1243 doi:10.1371/journal.ppat.1004583

1244 52. Balla KM, Lažetić V, Troemel ER. Natural variation in the roles of C. elegans autophagy components
1245 during microsporidia infection. PLOS ONE. 2019;14: e0216011. doi:10.1371/journal.pone.0216011

1246 53. Troemel ER, Félix M-A, Whiteman NK, Barrière A, Ausubel FM. Microsporidia Are Natural
1247 Intracellular Parasites of the Nematode Caenorhabditis elegans. Ward GE, editor. PLoS Biol.
1248 2008;6: e309. doi:10.1371/journal.pbio.0060309

1249 54. El Jarkass HT, Mok C, Schertzberg MR, Fraser AG, Troemel ER, Reinke AW. An intestinally secreted
1250 host factor limits bacterial colonization but promotes microsporidia invasion of C.
1251 elegans. bioRxiv. 2021; 2021.07.12.452088. doi:10.1101/2021.07.12.452088

1252 55. Mok CA, Au V, Thompson OA, Edgley ML, Gevirtzman L, Yochem J, et al. MIP-MAP: High-
1253 throughput mapping of Caenorhabditis elegans temperature-sensitive mutants via molecular
1254 inversion probes. Genetics. 2017;207: 447–463. doi:10.1534/genetics.117.300179

1255 56. Seidel HS, Ailion M, Li J, Oudenaarden A van, Rockman MV, Kruglyak L. A Novel Sperm-Delivered
1256 Toxin Causes Late-Stage Embryo Lethality and Transmission Ratio Distortion in C. elegans. PLOS
1257 Biology. 2011;9: e1001115. doi:10.1371/journal.pbio.1001115

1258 57. Bakowski MA, Desjardins CA, Smelkinson MG, Dunbar TL, Lopez-Moyado IF, Rifkin SA, et al.
1259 Ubiquitin-mediated response to microsporidia and virus infection in C. elegans. PLoS Pathog.
1260 2014;10: e1004200. doi:10.1371/journal.ppat.1004200

1261 58. A cullin-RING ubiquitin ligase promotes thermotolerance as part of the intracellular pathogen
1262 response in Caenorhabditis elegans | PNAS. [cited 12 Jun 2022]. Available:
1263 https://www.pnas.org/doi/10.1073/pnas.1918417117

1264 59. Yang W, Dierking K, Schulenburg H. WormExp: a web-based application for a Caenorhabditis
1265 elegans-specific gene expression enrichment analysis. Bioinformatics. 2016;32: 943–945.
1266 doi:10.1093/bioinformatics/btv667

1267 60. Lewis JA, Szilagyi M, Gehman E, Dennis WE, Jackson DA. Distinct patterns of gene and protein
1268 expression elicited by organophosphorus pesticides in Caenorhabditis elegans. BMC Genomics.
1269 2009;10: 202. doi:10.1186/1471-2164-10-202

1270 61. Helmcke KJ, Syversen T, Miller DM, Aschner M. Characterization of the effects of methylmercury
1271 on Caenorhabditis elegans. Toxicology and Applied Pharmacology. 2009;240: 265–272.
1272 doi:10.1016/j.taap.2009.03.013

1273 62. Eom H-J, Kim H, Kim B-M, Chon T-S, Choi J. Integrative Assessment of Benzene Exposure to
1274 Caenorhabditis elegans Using Computational Behavior and Toxicogenomic Analyses. Environ Sci
1275 Technol. 2014;48: 8143–8151. doi:10.1021/es500608e

1276 63. Menzel R, Menzel S, Swain S, Pietsch K, Tiedt S, Witczak J, et al. The Nematode Caenorhabditis
1277 elegans, Stress and Aging: Identifying the Complex Interplay of Genetic Pathways Following the
1278 Treatment with Humic Substances. Frontiers in Genetics. 2012;3. Available:
1279 https://www.frontiersin.org/article/10.3389/fgene.2012.00050

1280 64. Trzebny A, Slodkowicz-Kowalska A, Becnel JJ, Sanscrainte N, Dabert M. A new method of
1281 metabarcoding Microsporidia and their hosts reveals high levels of microsporidian infections in
1282 mosquitoes (Culicidae). Molecular Ecology Resources. 2020;20: 1486–1504.
1283 doi:https://doi.org/10.1111/1755-0998.13205

1284 65. Zhang G, Sachse M, Prevost M-C, Luallen RJ, Troemel ER, Felix M-A. A Large Collection of Novel
1285 Nematode-Infecting Microsporidia and Their Diverse Interactions with Caenorhabditis elegans and
1286 Other Related Nematodes. PLoS Pathog. 2016;12: e1006093. doi:10.1371/journal.ppat.1006093

66. Lange B, Kaufmann AP, Ebert D. Genetic, ecological and geographic covariables explaining host range and specificity of a microsporidian parasite. Journal of Animal Ecology. 2015;84: 1711–1719. doi:10.1111/1365-2656.12421

67. Bonneaud C, Tardy L, Giraudeau M, Hill GE, McGraw KJ, Wilson AJ. Evolution of both host resistance and tolerance to an emerging bacterial pathogen. Evolution Letters. 2019;3: 544–554. doi:https://doi.org/10.1002/evl3.133

68. Edgerton EB, McCrea AR, Berry CT, Kwok JY, Thompson LK, Watson B, et al. Activation of mosquito immunity blocks the development of transmission-stage filarial nematodes. PNAS. 2020;117: 3711–3717. doi:10.1073/pnas.1909369117

69. Grover M, Fasseas MK, Essmann C, Liu K, Braendle C, Félix M-A, et al. Infection of C. elegans by Haptoglossa Species Reveals Shared Features in the Host Response to Oomycete Detection. Frontiers in Cellular and Infection Microbiology. 2021;11: 973. doi:10.3389/fcimb.2021.733094

70. Osman GA, Fasseas MK, Koneru SL, Essmann CL, Kyrou K, Srinivasan MA, et al. Natural Infection of C. elegans by an Oomycete Reveals a New Pathogen-Specific Immune Response. Current Biology. 2018;28: 640-648.e5. doi:10.1016/j.cub.2018.01.029

71. Lansdon P, Carlson M, Ackley BD. Wild-type Caenorhabditis elegans Isolates Exhibit Distinct Gene Expression Profiles in Response to Microbial Infection. bioRxiv. 2021; 2021.10.16.464663. doi:10.1101/2021.10.16.464663

72. Wan YC, Troemel ER, Reinke AW. Conservation of Nematocida microsporidia gene expression and host response in Caenorhabditis nematodes. bioRxiv. 2022; 2022.06.15.496350. doi:10.1101/2022.06.15.496350

73. Mok CA, Au V, Thompson OA, Edgley ML, Gevirtzman L, Yochem J, et al. MIP-MAP: High-Throughput Mapping of Caenorhabditis elegans Temperature-Sensitive Mutants via Molecular Inversion Probes. Genetics. 2017;207: 447–463. doi:10.1534/genetics.117.300179

74. Dirksen P, Assié A, Zimmermann J, Zhang F, Tietje A-M, Marsh SA, et al. CeMbio - The Caenorhabditis elegans Microbiome Resource. G3: Genes, Genomes, Genetics. 2020;10: 3025–3039. doi:10.1534/g3.120.401309

75. Powell JR, Ausubel FM. Models of Caenorhabditis elegans Infection by Bacterial and Fungal Pathogens. In: Ewbank J, Vivier E, editors. Innate Immunity. Totowa, NJ: Humana Press; 2008. pp. 403–427. doi:10.1007/978-1-59745-570-1_24

76. Norris AD, Kim H-M, Colaiácovo MP, Calarco JA. Efficient Genome Editing in Caenorhabditis elegans with a Toolkit of Dual-Marker Selection Cassettes. Genetics. 2015;201: 449–458. doi:10.1534/genetics.115.180679

77. Stiernagle T. Maintenance of C. elegans. WormBook. 2006; 1–11. doi:10.1895/wormbook.1.101.1

78. Luallen RJ, Bakowski MA, Troemel ER. Characterization of Microsporidia-Induced Developmental Arrest and a Transmembrane Leucine-Rich Repeat Protein in Caenorhabditis elegans. PLOS ONE. 2015;10: e0124065. doi:10.1371/journal.pone.0124065

1324 79. Schindelin J, Arganda-Carreras I, Frise E, Kaynig V, Longair M, Pietzsch T, et al. Fiji: an open-source
1325 platform for biological-image analysis. Nature Methods. 2012;9: 676–682.
1326 doi:10.1038/nmeth.2019

1327 80. Langmead B, Salzberg SL. Fast gapped-read alignment with Bowtie 2. Nat Methods. 2012;9: 357–
1328 359. doi:10.1038/nmeth.1923

1329 81. Li H, Handsaker B, Wysoker A, Fennell T, Ruan J, Homer N, et al. The Sequence Alignment/Map
1330 format and SAMtools. Bioinformatics. 2009;25: 2078–2079. doi:10.1093/bioinformatics/btp352

1331 82. Garrison E, Marth G. Haplotype-based variant detection from short-read sequencing. 2012 [cited 4
1332 Jun 2022]. doi:10.48550/ARXIV.1207.3907

1333 83. Cook DE, Andersen EC. VCF-kit: Assorted utilities for the variant call format. Bioinformatics. 2017;
1334 btx011. doi:10.1093/bioinformatics/btx011

1335 84. Wang L, Wang S, Li W. RSeQC: quality control of RNA-seq experiments. Bioinformatics. 2012;28:
1336 2184–2185. doi:10.1093/bioinformatics/bts356

1337 85. Ewels P, Magnusson M, Lundin S, Käller M. MultiQC: summarize analysis results for multiple tools
1338 and samples in a single report. Bioinformatics. 2016;32: 3047–3048.
1339 doi:10.1093/bioinformatics/btw354

1340 86. Bray NL, Pimentel H, Melsted P, Pachter L. Near-optimal probabilistic RNA-seq quantification. Nat
1341 Biotechnol. 2016;34: 525–527. doi:10.1038/nbt.3519

1342 87. Marini F, Binder H. pcaExplorer: an R/Bioconductor package for interacting with RNA-seq principal
1343 components. BMC Bioinformatics. 2019;20: 331. doi:10.1186/s12859-019-2879-1

1344 88. Bakowski MA, Desjardins CA, Smelkinson MG, Dunbar TA, Lopez-Moyado IF, Rifkin SA, et al.
1345 Ubiquitin-Mediated Response to Microsporidia and Virus Infection in C. elegans. Schneider DS,
1346 editor. PLoS Pathog. 2014;10: e1004200. doi:10.1371/journal.ppat.1004200

1347 89. Chen K, Franz CJ, Jiang H, Jiang Y, Wang D. An evolutionarily conserved transcriptional response to
1348 viral infection in Caenorhabditis nematodes. BMC Genomics. 2017;18: 303. doi:10.1186/s12864-
1349 017-3689-3

1350 90. Eddy SR. Accelerated Profile HMM Searches. PLOS Computational Biology. 2011;7: e1002195.
1351 doi:10.1371/journal.pcbi.1002195

1352